

UNCLASSIFIED

AD NUMBER
AD824681
NEW LIMITATION CHANGE
TO Approved for public release, distribution unlimited
FROM Distribution authorized to U.S. Gov't. agencies and their contractors; Administrative/Operational Use; NOV 1967. Other requests shall be referred to Space and Missile Systems Organization, Los Angeles, CA 90045.
AUTHORITY
SAMSO USAF ltr, 28 Feb 1972

THIS PAGE IS UNCLASSIFIED

AD 824681

**TECHNICAL INFORMATION SERIES**

**R675D39**

STATEMENT OF UNCLASSIFIED

This document is subject to special export controls and each transmittal to foreign governments or foreign nationals may be made only with prior approval of *Space and Missile Systems Organization, attn: SMS/DI-STINFO, Los Angeles Air Force Station, California 90045*

**TRANSITION OF THE HYPERSONIC  
BOUNDARY LAYER ON A CONE**

**PART I - EXPERIMENTS AT  $M_{\infty} = 12$  AND 15**

**E. J. SOFTLEY  
B. C. GRABER  
R. E. ZEMPEL**

DEC 22 1967  
A

**SPACE SCIENCES  
LABORATORY**

**SPACE SCIENCES LABORATORY**  
EXPERIMENTAL FLUID PHYSICS SECTION

TRANSITION OF THE HYPERSONIC BOUNDARY LAYER  
ON A CONE:

PART I - EXPERIMENTS AT  $M_\infty = 12$  AND 15

by

E. J. Softley  
B. C. Graber  
R. E. Zempel

This work was performed for BSD, USAF under Contract AF 04(694)-772 and was declassified in accordance with instructions received October 24, 1967 from the Office of Information, Ballistic Systems Division, U. S. A. F.

Part of this paper was presented at the AIAA 6th Aerospace Sciences Meeting, January 1968 as paper No. 68-39.

R67SD39

November 1967

MISSILE AND SPACE DIVISION

GENERAL  ELECTRIC

## TABLE OF CONTENTS

	<u>Page</u>
Summary	iii
List of Figures	v
Notation	vii
1. INTRODUCTION	1
2. EXPERIMENTAL DETAILS	2
2.1 Shock Tunnel	2
2.2 Model and Flow Parameters	3
2.3 Surface Instrumentation	4
2.4 Probe Instrumentation	5
2.5 Flow Calibration and Computation	6
3. HEAT TRANSFER RESULTS	7
3.1 Detection of Transition	7
3.2 Heat Transfer Correlation	9
4. BOUNDARY LAYER PROFILE MEASUREMENTS	9
4.1 Pitot Pressure Results	9
4.2 Wedge Probe Results	10
4.3 Total Temperature Results	11
5. COMPARISON OF METHODS OF OBSERVATION OF TRANSITION	11

TABLE OF CONTENTS (Cont.)

	<u>Page</u>
6. TRANSITION RESULTS ON THE SHARP CONE	13
7.. TRANSITION RESULTS ON THE BLUNTED CONE	16
8. CONCLUSIONS	18
Appendix - Calculation of Boundary Layer Edge Properties for the Blunted Cone Flow Field	19
References	20
Tables	22

### Summary

The GE-SSL shock tunnel, fitted with a large contoured nozzle, has been used to observe transition of the boundary layer on a 12 ft., 5° cone. Free stream flow Mach numbers were 12 and 15 and were essentially uniform. Surface heat transfer distributions were obtained and these allow the definition of distinct laminar, transitional, and turbulent regions. Comparison is made also with measurements of the structure and thickness growth of the boundary layer. These observations were made with controlled variations in the wall temperature ratio, nose bluntness and unit Reynolds number. A discussion is presented of the influence of these parameters on transition and comparison made with recent results in other facilities.

### List of Figures

1. Sketch of large shock tunnel with contoured nozzle installed.
2. Sketch of 12° cone model in nozzle.
3. Detail of model construction.
4. Detail of surface instrumentation.
5. Detail of pitot probe assembly.
6. Pitot probe location in the boundary layer.
7. Detail of wedge probe.
8. Oscilloscope traces for pressure data.
9. Oscilloscope traces for heat gage data.
10. Typical pressure distributions along cone.
11. Edge Mach number distributions along cone.
12. Typical heat transfer distribution along cone.
13. Non-dimensional heat transfer along sharp cone (Conditions 1-5).
14. Non-dimensional heat transfer along sharp cone (Condition 6).
15. Non-dimensional heat transfer along sharp cone (Condition 7).
16. Non-dimensional heat transfer distribution along sharp cone (Conditions 8-9).
17. Heat transfer distributions along blunt cone.
18. Laminar heat transfer correlation.
19. Pitot pressure profiles across the boundary layer.
20. Non-dimensional pitot pressure profiles.
21. Wedge probe fluctuation across laminar boundary layer at  $X_B$ .

List of Figures (Cont.)

22. Total temperature across laminar boundary layer.
23. Velocity distribution across laminar boundary layer.
24. Total temperature as a function of velocity across laminar boundary layer.
25. Boundary layer thickness growth compared with heat transfer distribution.
26. Experimental observation of location of maximum disturbances.
27. Transition Reynolds Number as a function of unit Reynolds number.
28. Comparison of transition Reynolds numbers with results from other facilities.
29. Effect of local Mach number on transition Reynolds number.
30. Movement of transition location with increasing nose radius.
31. Transition Reynolds number as a function of nose Reynolds number.
32. Reynolds number, Mach number histories for three model nozzle configurations.
33. Transition location with respect to swallowing distances.

### Notation

$C_H$	Non-dimensional heat transfer rate (Stanton number)
D (IN)	Wedge Probe Dimension
M	Mach number
P (LB/IN <sup>2</sup> )	Pressure
q (BTU/FT <sup>2</sup> SEC)	Heat transfer rate
R (IN)	Radius
Re	Reynolds number
T (°K)	Temperature
U (FT/SEC)	Velocity
X (FT)	Distance along cone axis from virtual apex
Y (IN)	Radial distance from cone surface
δ (IN)	Boundary layer thickness

### Subscripts

B	at beginning of transition
c	cone
E	at end of transition
e	at edge of boundary layer
N	nose of model
R	recovery value
w	wall or surface value
SW	at location where boundary layer swallows nose induced entropy layer

0 total value  
5 reflected region of shock tunnel  
∞ ahead or outside of cone shock

Superscript

' behind normal shock

## 1. INTRODUCTION

The observation of a boundary layer, as it undergoes transition from laminar to turbulent state, has been made extensively at subsonic and supersonic speeds. Recently, attention is given to the phenomena at hypersonic conditions. As will be seen later the transition Reynolds number increases rapidly with local Mach number and very quickly outstrips typical, continuous wind tunnel capability. Two ways to circumvent the problem are possible. Firstly helium, instead of air can be used as a test gas. The lower condensation temperatures allow the use of much lower free stream static temperatures and, through the attainment of higher densities, provides larger Reynolds numbers for any given Mach number. This approach was used by Maddalon and Henderson (1) to successfully observe transition in Helium at local Mach numbers as high as 15.8.

Alternatively, a physically large facility can be used allowing a model sufficiently large that transition can be observed in air. The GE-SSL 6"/54" shock tunnel has a nozzle which is 54" exit diameter and some 22 ft. long. This allows the use of a slender cone long enough that transition can be observed over a range of conditions, at free stream Mach numbers up to 15, with corresponding local Mach numbers ( $M_e$ ) up to 12.

The detection of transition can be accomplished in several ways. A method used extensively by Nagamatsu (5) observes the increase of heat transfer to the surface as transition occurs. Similarly for the studies here, the surface heat transfer is again observed at a variety of flow conditions. From this the observation of the beginning and end of transition are reported.

In addition, probe measurements within the boundary layer detect the change of the structure and boundary layer thickness growth and these are compared with the surface heat transfer measurements.

## 2. EXPERIMENTAL DETAILS

### 2.1 Tunnel and Nozzle

The GE 6"/54" shock tunnel has been described in earlier literature (see refs. 2 and 3). Modification of the tunnel with a parallel flow contoured nozzle is described in ref. 4. The nozzle has been designed for a uniform flow free stream Mach number of 20. However, it has been operated satisfactorily down to a Mach number of 10. For the studies shown here a number of conditions have been calibrated at two Mach numbers (nominally 12 and 15). The method of calibration and the accuracy is discussed in a later section. The tunnel is operated in a reflected mode, the gas behind the reflected shock at the end of the shock tube being used as the hot gas source for the nozzle expansion. Fig. 1 shows a general layout of the shock tunnel.

Tailored operation of the tunnel is not used and a wide range of conditions can be produced. The pressure and temperature in the reflected region generally decay with time in a manner shown in fig. 8. For convenience the data is usually obtained for any one run by taking the point in time when the  $P_5$  or reflected region pressure reaches a pre-determined value for that test condition. In this manner, the flow conditions become very repeatable in that the only remaining reflected region variable is the total temperature. In general, the total temperatures scatter about the nominal value by  $\pm 100^\circ\text{K}$ .

The resulting run to run variation in flow is usually too small to significantly affect the data and the repeatability of heat transfer distributions has been excellent. This can be seen, for example, in fig. 12.

Traces for  $P_5$ , the reflected region pressure,  $P_c$ , the cone surface pressure and  $P_o^1$ , a pitot probe pressure are shown in fig. 8. From these and the heat transfer traces in fig. 9 it is possible to conclude that the cone boundary layer reaches a quasi-steady state condition ( $P_c/P_5$  constant etc.) in the same time period taken to establish a quasi-steady free stream. Comments on the steadiness of the transition phenomenon will be made in section 3.

## 2.2 Model and Parameter Variations

The model used for these tests was a 12 ft. long,  $5^\circ$  half angle cone. It is made of aluminum in sections which bolt together and has a final surface finish of approximately 40 micro inches. Local skin thicknesses are typically 1/2 inch. The nose sections are interchangeable and nose radii from .001 inch to 1 inch have been tested. The location of the model in the nozzle is shown in fig. 2. The model surface temperature is that of the environment before testing, namely room temperature, and because of the short duration of the flow does not change.

By operating the shock tunnel with different reflected region temperatures a range of wall temperature ratios  $\frac{T_w}{T_o}$  from .12 to .26 were obtained. In addition for any given reflected region temperature, unit Reynolds number changes can be obtained by varying the reflected region pressure. As mentioned earlier, two free stream Mach numbers can be obtained by varying the throat diameter of the contoured nozzle.

### 2.3 Surface Instrumentation

The instrumentation installed in the surface of the model consists of heat gages and pressure transducers. Figs. 3 and 4 show some of the details of the construction. Instrumentation blocks which plug into the model are used and the instrumentation is installed in these blocks. The surface heat gages are thin film gages painted onto quartz substrats. Details of the construction and calibration has been described earlier in ref. 4. The pressure transducers used were Shaevitz-Bytrex HFD 15 gages which use semi-conductor strain gage elements. The devices have an advantage in that they are very insensitive to acceleration and therefore unaffected by vibration of the model.

The general philosophy behind all instrumentation is that a first stage amplifier be located very close to the transducer. This generally minimizes excess electronic noise and keeps the component of the circuit which has very low level currents physically as small as possible. Hence, in fig. 4 a circuit board is mounted on the back of each instrumentation block. The heat gage amplifier has been described in ref. 4. The pressure gage amplifier uses a transistorized bridge circuit.

The heat gages are installed on a single ray of the cone surface and in general this ray is the top ray on the model as installed in the tunnel. This minimizes erosion of the gages due to dust etc. from the reflected region of the tunnel. Hence, any heat transfer distribution obtained is obtained along a single ray. No attempt was made to observe circumferentially on the model.

#### 2.4 Probe Instrumentation

In addition to the surface measurements details of the structure of the boundary layer, laminar through turbulent, were obtained using various probe assemblies. A typical one is shown in fig. 5 where a pitot pressure probe assembly is shown. This observes the local stagnation pressure through a boundary layer and fig. 6 shows a typical geometry during an experiment. Typical probe tip diameters were .060 inches as shown and the individual probes are separated to minimize interference from reading to another. Of course, no surface measurements are attempted downstream of such a probe. Piezo-electric pressure transducers were used and field effect transistor amplifiers of a type described in ref. 4 installed in the probe housing.

In addition, total temperatures were observed using pulse heated fine wire probes and details of this experiment are more adequately covered in ref. 6. The probe assembly shown in fig. 5 can also be fitted with small wedge probes. Each wedge has a small heat gage located on it close to the leading edge. A sketch is shown in fig. 7. The heat gage which operates in local flows described by the strong interaction theory sees free stream fluctuations whose wave length is large compared with the characteristic probe dimension  $D$  as variations in its local free stream and responds accordingly. There is a decrease in gage response at high frequencies due to the nature of the gage itself but the instrumentation has been used to observe the nature of disturbances within the boundary layer. Observations have also been made in the free stream.

## 2.5 Flow Calibration and Computation

The calibration of flows in a nozzle such as described earlier is generally accomplished using total pressure rake assemblies in the tunnel with no model present. When the nozzle is operated below design Mach number a continuing expansion takes place in the nozzle such that flow variations occur axially and radially in such a nozzle. These have been obtained for the nozzle on the GE shock tunnel, with typical experimental scatter. The surface pressure measurements made with the transducers described earlier have proven to be much better in quality and hence, for the flows described here these surface pressure measurements have been the principal measurements used to describe the flows in the tunnel. Typical cone pressure data is shown in fig. 10. A pressure distribution is drawn through the data. The surface pressure is known locally (and local means X, the axial position) and the total pressure known in the reflected region and it is possible to compute free stream and local edge properties. The assumption is made that the flow is that of a local infinitesimal ideal cone. Dimensions across the shock layer are ignored. Hence, a local edge property refers to the quoted X whilst a local free stream property would really refer to a point somewhat upstream of the quoted X.

As a check on this process, the stagnation pressure is considered at both the edge of the boundary layer and in the free stream (see for example fig. 21). The result is also shown in fig. 10 where stagnation pressure values obtained by the calculation that produces the edge Mach number are

compared with the measured values. The agreement is sufficient that the process computes local edge Mach numbers within  $\pm .05$  with a fair degree of confidence.

By making these measurements of surface pressure on the sharp cone at all flow conditions, it is possible to produce a set of calibrated flow conditions and these have been quoted in Table I. For the sharp cone, a set of local edge Mach numbers is shown in fig. 11. For the blunted cone surface pressure measurements were also obtained. The blunt body flows are calculated using the GE VIZAAD computer program (8) and a brief discussion of the details of this program are in Appendix A. The free stream properties obtained from the sharp cone measurements were used as input to the blunt cone calculations.

### 3. HEAT TRANSFER RESULTS

#### 3.1 Detection of Transition

The surface heat gages allow the determination of heat transfer as a function of axial distance along the model. The distribution of heat transfer for a boundary layer which starts laminar and undergoes transition to turbulence along the model is shown typically in fig. 12. The laminar heat transfer declines from a high value near the nose and reaches a minimum when transition begins, reaching a mathematical maximum at the end of the transition region. Hence, as shown in fig. 12 it is possible to pick out two distinct points which, based on the heat transfer, can be described as the beginning and end of the transition region. Such points are more clearly defined if the data throughout each region is used. For example, in fig. 13

where logarithmic plots of the heat transfer are shown, it is possible to draw straight lines through each portion of the data and the intersection of the straight lines defines the points.

The data shown in fig. 12 is for one given flow condition and for three separate runs for the shock tunnel. For each run readings are taken at a point in time corresponding to the same pressure level  $P_5$  and the data repeats extremely well. In fact the location of transition must repeat from run to run in order for the data to reproduce as well as shown in fig. 12. This suggests that any parameter which can influence transition but is not directly observed, for example, free stream turbulence is repeatable from run to run.

For some of the flow conditions, a very careful check was made on the change in the heat transfer distribution with time. The pressure level  $P_5$  does decay as does  $T_5$  and there is a resulting slight change in the unit Reynolds number. It was found that if heat transfer distributions were calculated for intervals of time during any given run the movement of transition was exceedingly slight and in fact could hardly be detected within normal scatter of the data. It is concluded that the transition phenomena is steady in time during the flow and establishes within the time taken to establish the boundary layer flows themselves.

At different flow conditions the change in the observed heat transfer distribution is demonstrated in fig. 13. For convenience the non-dimensional heat transfer or Stanton number is shown against a Reynolds number and there is a distinct movement of the transition point. The heat transfer

distributions observed at other flow conditions are shown in figs. 14 through 16 for the sharp cone. In general, the detection of transition is easily made from the heat transfer distribution. In fig. 17 some non-dimensional heat transfers are shown for various nose bluntnesses and there is a distinct movement back of transition with increasing nose bluntness for the range of nose bluntnesses used for these tests.

### 3.2 Heat Transfer Correlations

Since this paper is primarily concerned with the observation of transition, discussion of the heat transfer data itself will be left to another paper (see ref. 7). However, some degree of confidence that the laminar heat transfer so called is indeed laminar is needed before any definite statements on transition could be made. Fig. 18 shows a plot of variously selected laminar heat transfer points where "laminar" is defined as being ahead of  $X_B$  as in fig. 12. The data is compared to the Eckert correlation (18). As can be seen, the laminar heat transfer is easily recognizable as being at the levels that one would expect. The remaining error is probably that of this experiment.

## 4. BOUNDARY LAYER PROFILE MEASUREMENTS

### 4.1 Pitot Pressure Results

The pitot pressure rake assembly described earlier has been used to obtain the variation of pitot or stagnation pressure from the surface of the wall out to the free stream. A typical set of results is shown in fig. 19 where for one particular flow condition the profiles at 3, 5, 7 1/2, and 9 ft. respectively are shown. The boundary layer thickness increases with axial

distance in a manner discussed later. The structure also changes and this is best seen if the data as shown in fig. 19 is reduced to the non-dimensional form shown in fig. 20. The total pressure is non-dimensionalized with respect to boundary layer thickness. For this purpose the  $\delta$  is chosen from the pitot pressure probe results. It was found that it was possible to overlay data obtained in laminar or turbulent regions. The structural change from laminar through turbulent does provide an alternate means of detection of transition. A comparison between the two is shown later. It is possible from the results shown to compute the Mach number distribution through the boundary layer, and providing some information is known about the total temperature, it is possible to compute other variables through the boundary layer. An analysis of the boundary layer structure so obtained will be made in future reports.

#### 4.2 Wedge Probe Results

The wedge probe version of the boundary layer rake assembly as described earlier uses miniature wedges with surface heat gages to detect disturbance levels in the boundary layer. The results are demonstrated in fig. 21 where the non-dimensional output of the gages is shown for this purpose. The fluctuations of each wedge probe is non-dimensionalized with respect to its mean steady state value as shown. This steady state value varies across the boundary layer and indeed is a way of observing the structure of the boundary layer. The non-dimensional disturbances appear to peak at a location  $3/4$  of the boundary layer thickness away from the wall. This represents a somewhat crude observation of boundary layer

disturbances compared with low velocity hot wire studies and as yet provides little extra information with respect to the transition phenomena at hypersonic conditions.

#### 4.3 Total Temperature Profiles

In order to obtain velocity profiles from the pitot pressure profiles described earlier it is necessary to have one other important thermodynamic variable, for example, the total temperature. A technique using pulse heated fine wire probes described in ref. 6 has been employed here and from this it was possible to obtain the total temperature and hence the velocity through the boundary layer. An example for the laminar boundary layer is demonstrated in fig. 22. When this is combined with a suitable total pressure distribution, it is possible to obtain the velocity profile shown in fig. 23. The relationship between the total temperature and velocity is calculated at intervals through the boundary layer and compared with the well known Crocco integral (20) in fig. 24. As can be seen, the total temperature is not adequately described by the Crocco integral through the laminar boundary layer studies here. The total temperature profiles have not yet been obtained in the turbulent boundary layer and hence the results relevant to transition phenomena are incomplete. Results of Danberg (19) for a turbulent boundary layer are shown for comparison in fig. 24 and appear closer to the Crocco relationship.

#### 5. COMPARISON OF METHODS OF OBSERVATIONS OF TRANSITION

The surface heat transfer distribution as shown earlier is used to define the beginning and end of transition. A comparison can be made between

this method and that using boundary layer thickness or total pressure measurements. As mentioned earlier, the stagnation pressure profile measurements can be used to obtain a boundary layer thickness and an evaluation of this thickness for one tunnel flow condition is shown in fig. 25 where the boundary layer thickness is shown on the same scale and for the same condition as the heat transfer distribution. The departure of the boundary layer growth from laminar to turbulent correspond very closely to the surface heat transfer departure from laminar to turbulent. This suggests that a shadowgraph picture which observes transition by observing the structure change and thickness growth of the boundary layer should give a beginning of transition comparable to that observed from the surface heat transfer measurements.

It is also possible, by comparing the profile structure in fig. 20, to see that the structure of the laminar boundary layer, as defined by total pressure measurements is unchanged up to the point where transition begins (in this case 4 1/2 ft. from the cone tip). At 7 1/2 ft. the flow appears turbulent and the total pressure distribution does not change from 7 1/2 to 9 ft. Fully developed turbulent flow has been achieved and, for comparison, turbulent flow at a different location, for a higher free stream Reynolds number, is shown to also correlate very well. Observations of boundary layer transition by using a small pitot probe located about midway through the boundary layer should also allow the determination of the same point of transition and this was the technique used by Maddalon and Henderson (1) in the NASA Langley Helium Tunnel.

Micro-structure measurements in the transitioning boundary layer are difficult to achieve at hypersonic Mach numbers. The wedge probe has allowed a crude observation of this. The wedge has been used to observe the disturbances across the boundary layer and the location of the maximum disturbances can be located within the boundary layer. However, one complete profile only exists for the location of transition. This was made at 4 1/2 ft. in the sharp cone, at condition 3, for which the earlier boundary layer growth observations were made (see fig. 21). The location of peak disturbance is about 3/4 of the boundary layer thickness from the wall. This is compared with data from other sources in fig. 26. Notice that the black points represent data observed at the beginning of transition  $X_B$ . To compare this with earlier data, for example that shown in Potter and Whitfield (9) it should be observed that much of this earlier data was obtained with hot wires where the location of disturbances was often in the laminar boundary layer ( $X < X_B$ ). Maddalon and Henderson's experiments at high shock numbers show disturbances which peak in the outer edge of the laminar boundary layer. These disturbances grow, with the location of the peak moving inward towards the wall, such that at the location of transition  $X_B$  the peak disturbances are at  $Y/\delta = .75$ . Hence, it must be observed that the beginning of transition as observed by surface heat transfer and boundary layer growth would be different for that where the micro-structure of the boundary layer was closely observed.

#### 6. TRANSITION RESULTS ON THE SHARP CONE

The transition data obtained at Mach 10 and 12 is shown in fig. 27

where the transition Reynolds number at the location of transition ( $Re_{x_B}$ ) is considered a function of the free stream unit Reynolds number. The open symbols represent data obtained in this study at a wall temperature ratio of .26 with the Mach number at transition essentially constant at  $10.2 \pm .2$ . An increase of unit Reynolds number gives an increase of transition Reynolds number with the data approximating  $Re_{x_B} \propto (Re/Ft.)^3$ . A similar effect is observed with Mach 12.2 with insufficient data to draw an accurate trend. Note that at Mach 10.2,  $\frac{T_w}{T_R} = .26$  the unit Reynolds number variation is obtained by density variation only; the free stream and local velocities being essentially constant.

Changing the free stream total temperature,  $T_o$ , changes the wall temperature ratio  $\frac{T_w}{T_R}$  and it is found that the data agrees with the previously determined relationship. The one exception is a condition for which the total temperature is  $3000^\circ K$ . For this case the local Mach number is 9.7. Simple correction for the Mach number shows that this point when corrected to 10.2 agrees with the correlation of the other data. Measurements in other facilities have observed a unit Reynolds number effect similar to the above (10, 11). It is concluded that variations in the wall temperature ratio do not affect transition, a fact that has been observed by some other observers. Confining ourselves to cone data only, Sanator, DeCarlo and Torillo (12) have also observed at a local Mach number of 8.8, a lack of effect of wall temperature on transition. In their case the wall temperature was varied by varying the surface temperature, with the stagnation temperature of the tunnel remaining constant. Stetson and

Rushton (13) did observe an effect of wall temperature, however, at a local Mach number of 4.8. There have been other observations concerning this effect of wall temperature on transition, notably on flat plates and these have given conflicting results. Deem and Murphy (14) note no effect of wall temperature while Richards and Stollery (15) detect a very strong and definite effect of wall temperature on transition. At this point in time it is not possible to determine why these observations are different.

In fig. 28 data from other facilities is shown and it can be observed that there is a general increase in transition Reynolds number with increasing Mach number. Fig. 29 shows the effect of local Mach number on transition Reynolds numbers and is obtained from the data of fig. 28 by assuming that data obtained at the same unit Reynolds number in different facilities is comparable. This is, however, no physical argument to substantiate this step. Hence, fig. 29 should be regarded with caution. No significance to the exact trend can be assumed until the phenomena, "unit Reynolds number", is understood. The data is restricted to cone flows, sufficiently sharp that the free stream Reynolds number based on nose radius,  $Re_{\infty N} < 200$ . For comparison the Mach number curve of Sheetz (16) obtained from data from a firing range is shown for comparison. The data obtained from the range produces a curve of type  $Re_{x_B} \propto M^{3.5}$ . (This is, however, a comparison with various wall temperatures and nose bluntnesses). The shock tunnel data compares closely, at high Mach numbers, to a similar relationship with a selected power law variation shown for comparison only.

There is data by Nagamatsu (5), in a conical nozzle shock tunnel, which shows a very different Mach number effect on transition. It is not shown on fig. 29 because it is impossible to isolate any influence of variations in unit Reynolds number. The "beginning of transition" as quoted by Nagamatsu agrees with the transition Reynolds numbers shown in fig. 29 (tunnel data) at local Mach numbers about 10 but produces much lower transition Reynolds numbers at higher local Mach numbers. This is almost certainly a result of the severe axial gradient of Mach number and pressure in the conical flow facility.

#### 7. TRANSITION RESULTS ON THE BLUNTED CONE

The SSL results all shown so far have nose radius of .001 on the 12 ft. cone model. This is considered sharp. If the nose radius is increased then transition on a blunted cone can be observed. A typical trend is shown in fig. 30 where the location of the beginning of transition  $X_B$  as  $R_N$  is increased is shown for two flow conditions. There is a general increase in transition distance  $X_B$  as the nose radius increases. The local Reynolds number at transition also changes but less strongly. For comparison in fig. 30 the location of the swallowing distance as nose radius is increased is shown. In this instance the swallowing distance is defined as the distance to achieve 95% of the final asymptotic edge Mach number. Hence, the swallowing distance is not exactly that defined by Stetson and Rushton but is sufficiently close that for the influence shown here is accurate enough. The general observation is made that the transition moves back as the swallowing distance for all observed cases. Hence,  $\frac{X_B}{X_{SW}} > 1$ , defined by

Stetson and Rushton (13) as sharp. (In defining the different regions of nose bluntness on transition, Stetson and Rushton regarded  $\frac{X_B}{X_{SW}}$  is an independent parameter).

The data shown in fig. 30 and all other data obtained can all be correlated on a single curve shown in fig. 31 with the free stream, nose radius, Reynolds number as independent parameter. For  $M_e \approx 10$  the curve appears to be asymptotic at low  $Re_{\infty N}$  to about  $Re_{x_B} = 5 \times 10^6$  for the data shown. Notice that this data is all obtained for local Mach number of about 10.2 and has all been adjusted for slight differences in free stream unit Reynolds number. It is noted that the effect of the nose is sufficiently strong, that the Reynolds number is doubled as  $Re_{\infty N}$  increases from  $10^2$  to  $10^5$ . Hence, the conclusion in ref. 13 that for  $\frac{X_B}{X_{SW}} > 0.4$  the transition  $Re_{x_B}$  may be considered equal to the sharp limit certainly does not apply to the trends observed here. Indeed it would appear that  $\frac{X_B}{X_{SW}}$  is a parameter only in the sense that it has limited variations, i. e. almost invariant as nose bluntness changes.

It is possible to produce a curve similar to fig. 10, ref. 13 (see fig. 33) which demonstrates the movement of transition as a function of  $\frac{X_B}{X_{SW}}$ . In this region the movement of transition back with increased nose radius (decreasing  $\frac{X_B}{X_{SW}}$ ) is no different from that observed earlier by Potter and Whitfield (9).

Since blunting the nose increases  $X_B$  there is only a limited range of free stream stagnation temperatures for which transition is observed on the cone in this facility. Decreasing the wall temperature ratio from .26 to .21

no effect on transition beyond the scatter of the data could be observed.

It is interesting to observe, as shown in fig. 32 the overall effect of the blunt nose on the cone flows. The histories of Reynolds number versus Mach number for the sharp and a blunt cone are shown and their relationship to the Reynolds number, Mach number "transition criteria" curve (see fig. 29). The blunted cone history shows a lower Mach number earlier on the cone, however, transition is sufficiently delayed that the local Mach number is not significantly different from that of the sharp. In fact a new criteria for this blunt cone with  $Re_{x_B}$ , increased from the relationship shown in fig. 31 is necessary. In fact it is apparent that this must be so since the "criteria" curve for the sharp cone intercepts the blunt cone history at about 3 ft. whereas transition has occurred at 8 ft.

It is also interesting to observe the Mach number, Reynolds number history on a  $5^\circ$  cone when installed in a conical nozzle as is the cone of Nagamatsu, et al (5, 20). As can be seen in fig. 32 the rapid drop in density due to the continued strong expansion of external flow results in the local unit Reynolds number also decreasing. The net result is that the local Reynolds number becomes almost constant near the end of the cone making it almost impossible for transition to occur there.

## 8. CONCLUSIONS

Transition at local Mach numbers of 10 and 12 has been observed on a 12 ft. cone model in the GE-SSL shock tunnel. Transition is readily detectable from heat transfer rate measurements and appears repeatable from run to run of the facility. A unit Reynolds number effect similar to

that observed in other facilities was observed in this facility. Correlating data with that from various facilities it was found that for a sharp cone the effect of local Mach number on transition was extremely strong, typically  $Re_{xP} \propto M^4$ . In common with some other observations the data obtained for different wall temperature ratios seems to correlate on the same unit Reynolds number curve suggesting an invariance of transition location to wall temperature ratio. In addition small nose bluntness of the model moves the transition point back such that it stays behind the swallowing distance, resulting in an increase of local Reynolds number with bluntness.

#### Appendix

##### Calculation of Boundary Layer Edge Properties For Blunted Cone Flow Field

These flow fields were calculated using an existing GE-RSD Computer Program (8). A summary only of the method will be given here.

The shock shape in the vicinity of the nose is calculated from the method of Gravalos et al (17). This allows the calculation of the entropy at any streamline after it passes through the nose induced shock. A mass balance is used to find where on the cone surface this streamline is at the edge of the boundary layer. Flow was assumed isentropic along streamlines within the shock layer. Experimental surface pressure measurements were used as a second thermodynamic input. Boundary layer thickness and displacement thickness were calculated from expressions developed by Walker. An iteration process is needed because of coupling between the various equations.

## References

1. Maddalon, D. V. and Henderson, A., Jr., "Boundary Layer Transition at Hypersonic Mach Numbers", AIAA Paper 67-130, Jan. 1967.
2. Warren, W. R., Kaegi, E. M., Harris, C. F. and Geiger, R. E., "Shock Tunnel Studies of the Aerodynamics of Atmospheric Entry", GE TIS R62SD56, 1962.
3. Warren, W. R., "Design and Performance of the G. E. 6" Shock Tunnel Facility", Proceedings of 1st Shock Tube Symposium, SWR-TM-57-2, Feb. 1957.
4. Softley, E. J. and Graber, B. C., "Techniques for Low Level Pressure and Heat Transfer Measurements and Their Application to Base Flows", GE TIS R67SD2.
5. Nagamatsu, H. T., and Sheer, R. E., Jr., "Hypersonic Laminar Boundary Layer Transition on 8 ft.  $10^\circ$  Cone,  $M_i = 9.1-16$ ", AIAA Report 66-494.
6. Softley, E. J., "Use of a Pulse Heated Fine Wire Probe for the Measurement of Total Temperature in Shock Driven Facilities", GE TIS (In Preparation).
7. Graber, B. C., Weber, H. E. and Softley, E. J., "Comparison of Laminar and Turbulent Cone Boundary Layer Flow With and Without Pressure Gradient", GE TIS R67SD49.
8. Studerus, C. J. and Dienna, E. A., "Viscous Interaction Zero Angle of Attack (VIZAAD) Program", GE-MSD TIS 64SD292, Nov. 1964.
9. Potter, J. L. and Whitfield, J. D., "Effect of Slight Nose Bluntness and Roughness on Boundary Layer Transition in Supersonic Flows", Journal of Fluid Mechanics, Vol. 12, Pt. 4, pp. 501-535, April, 1962.
10. Stainback, P. C., "Some Effects of Roughness and Variable Entropy on Transition at a Mach Number of 8", AIAA Paper 67-132, Jan. 1967.
11. McCauley, W. D., Saydah, A., and Bueche, J., "The Effect of Controlled Three Dimensional Roughness on Hypersonic Laminar Boundary Layer Transition", AIAA Paper No. 66-26.

12. Sanator, R. J., DeCarlo, J. P. and Torrillo, D. T., "Hypersonic Boundary Layer Transition Data for a Cold-Wall Slender Cone", AIAA Journal, pp. 758-760, April 1965.
13. Stetson, K. F. and Rushton, G. H., "A Shock Tunnel Investigation of the Effects of Nose Bluntness, Angle of Attack and Boundary Layer Cooling on Boundary Layer Transition at a Mach Number of 5.5", AIAA Paper No. 66-495.
14. Deem, R. E. and Murphy, J. S., "Flat Plate Boundary Layer Transition at Hypersonic Speeds", AIAA Paper No. 65-128, Jan. 1965.
15. Richards, B. E. and Stollery, J. L., "Transition Reversal on a Flat Plate at Hypersonic Speeds", AGARDograph No. 97, May 1965.
16. Sheetz, N. W., Jr., "Boundary Layer Transition on Cones at Hypersonic Speeds", AIAA Report 67-131.
17. Gravalos, F. G., Edelfelt, I. H., and Emmons, H. W., "The Supersonic Flow Field About a Blunt Body of Revolution for Gas at Chemical Equilibrium", Proc. 9th Annual Congress IAF, Aug. 1958.
18. Eckert, E. R. G., "Engineering Relations for Friction and Heat Transfer to Surfaces in High Velocity Flow", Journal of Aeronautical Sciences, pp. 585-587, August 1955.
19. Danberg, J. E., "Characteristics of the Turbulent Boundary Layer With Heat and Mass Transfer at  $M = 6.7$ ", NOL TR 64-99, Naval Ordnance Laboratory.
20. Nagamatsu, H. T., Graber, B. C. and Sheer, R. E., "Roughness, Bluntness, and Angle-of-Attack Effects on Hypersonic Boundary-Layer Transition", Journal Fluid Mechanics, Vol. 24, pp. 1-31, 1966.

TABLE 1

FREE STREAM CONDITIONS AT X = 0

Cond.	$P_5$ lbs/in <sup>2</sup>	(Nominal) $T_5$ °K	$M_\infty$	$\dot{J}_\infty$ lbs/ft <sup>3</sup> $\times 10^4$	$u_\infty$ ft/sec	$P_\infty$ psi. $\times 10^2$	$T_\infty$ °K	$\frac{\rho_\infty u_\infty}{\mu_\infty}$ Re/ft $\times 10^{-6}$
1.	4000	1400	11.50	9.1	5766	3.50	57.8	2.0
2.	2500	1400	11.40	5.65	5703	2.21	58.4	1.22
3.	1500	1400	11.35	3.95	5672	1.57	59.5	0.84
4.	1000	1400	11.25	2.13	5645	0.83	58.0	0.46
5.	500	1400	11.20	1.29	5632	0.50	58.2	0.28
6.	4000	2300	11.00	5.05	7569	3.68	108.9	0.75
7.	3000	3000	10.40	2.84	8775	3.13	164.1	0.36
8.	4000	1400	14.85	2.64	5808	0.62	35.2	1.07
9.	2400	1400	14.70	1.73	5754	0.41	35.2	0.67
10.	5000	1900	11.40	7.49	6844	4.17	82.9	1.32
11.	3000	1900	11.25	4.76	6776	2.61	83.6	0.83
12.	1000	1900	11.20	1.60	6710	0.89	81.3	0.27
13.	5000	1900	14.70	2.18	6896	0.74	50.6	0.68
14.	6000	1400	15.00	3.75	8713	0.86	34.5	1.50

TABLE 2  
SHARP CONE TRANSITION DATA

Condition	$X_B$ Feet	$X_E$ Feet	$M_{\bullet B}$	$M_{e B}$	Re/ft $\times 10^{-6}$	$Re X_B$ $\times 10^{-6}$	$T_w/T_R$	$Re_{\bullet N}$
1	2.25	4.0	11.9	10.1	2.56	5.7	.26	200
2	3.4	5.8	11.9	10.1	1.55	5.3	.26	120
3	4.5	6.5	12.1	10.2	0.95	4.3	.26	80
4	6.7	11.0	12.2	10.3	0.62	4.1	.26	45
5	11.0	-	12.4	10.5	0.30	3.2	.26	23
6	4.5	7.5	11.7	10.0	1.01	4.56	.16	80
7	7.4	11.0	11.4	9.7	0.38	2.8	.12	30
8	8.7	-	15.3	12.2	1.40	12.2	.25	110
9	12.0	-	15.6	12.4	0.86	10.6	.25	70
10								
11	3.7	5.7	11.9	10.1	1.18	4.4	.21	100
12	10.0	-	12.4	10.4	0.35	3.5	.21	30
13	9.8	-	15.5	12.2	1.16	11.4	.21	90
14	7.7	10.5	15.4	12.3	1.8	13.7	.25	140

TABLE 3

BLUNTED CONE TRANSITION DATA

$R_N$ inches	Cond.	$X_B$ Feet	$X_E$ Feet	$M_e B$	$Re/ft$ $\times 10^{-6}$	$Re_{\infty}/ft$ $\times 10^{-6}$	$Re \times B$ $\times 10^{-6}$	$T_w/T_R$	$Re_{\infty} N$
0.1	1	4.0	5.2	9.9	1.96	1.8	7.9	.26	16,500
	2	5.6	7.7	10.1	1.23	1.1	6.9	.26	10,000
	3	7.5	-	10.2	0.76	0.67	5.7	.26	6,200
0.172	10	4.4	6.4	9.9	1.38	1.3	6.1	.21	13,000
	11	7.2	-	10.1	0.82	0.81	5.9	.21	7,700
0.30	1	4.9	8.2	9.8	1.81	1.7	8.9	.26	29,000
	2	6.5	9.8	10.1	1.14	1.0	7.4	.26	17,000
	3	8.0	-	10.2	0.71	0.66	5.7	.26	10,500
0.50	10	5.7	8.7	9.9	1.25	1.3	7.2	.21	22,000
	11	9.7	-	10.2	0.75	0.81	7.3	.21	13,000
0.30	1	8.3	11.6	9.6	1.24	1.6	10.3	.26	50,000
	2	9.5	-	10.2	0.95	1.0	9.0	.26	30,000
0.50	1	12.0*	-	8.6	0.84	1.5	10.0	.26	82,000
1.00	1	12.0*	-	5.6	0.5	1.5	2.4	.26	160,000

\* Laminar flow on cone. Flow properties given at end of cone.

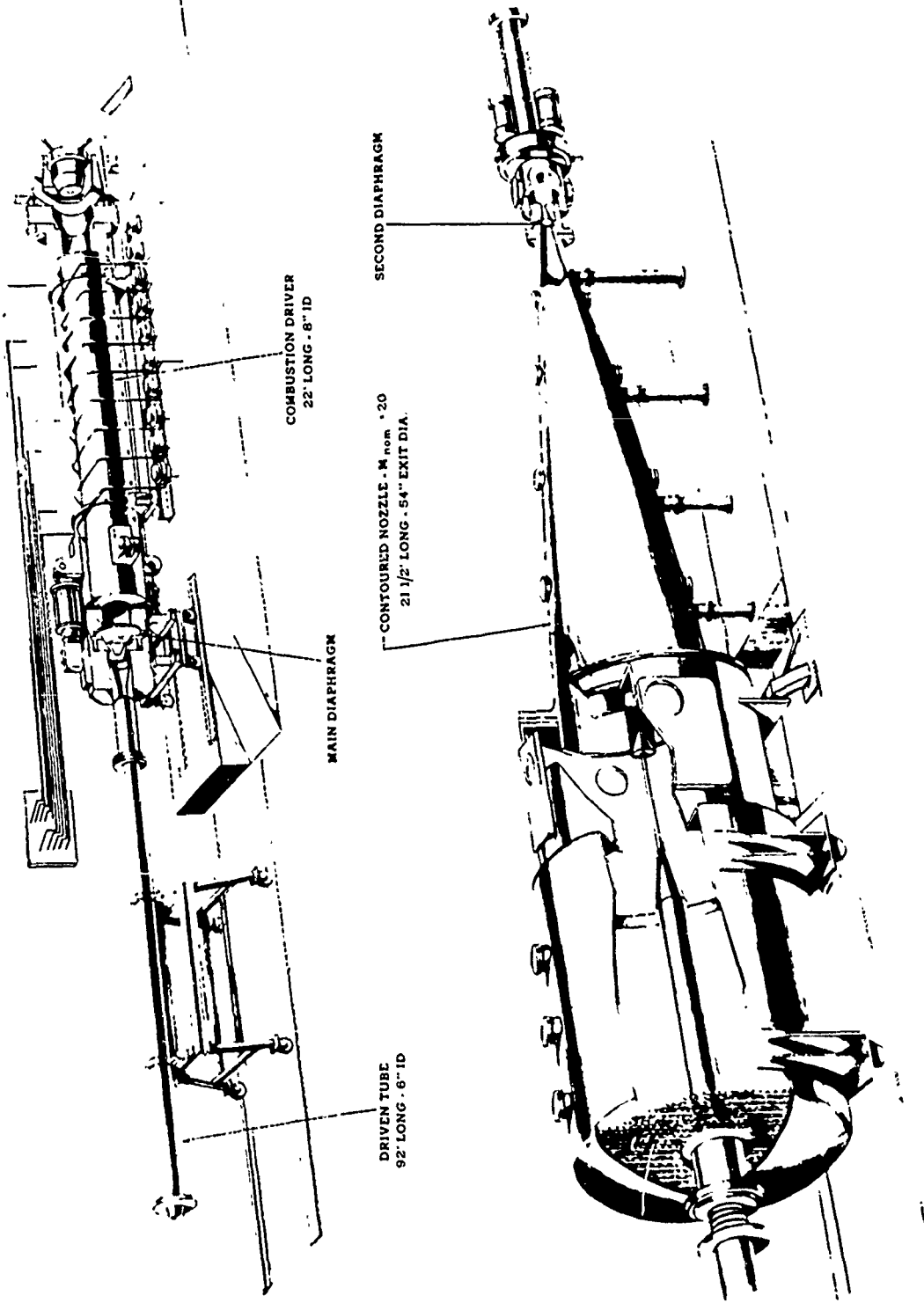


Figure 1  
SKETCH OF LARGE SHOCK TUNNEL WITH CONTOURED NOZZLE INSTALLED

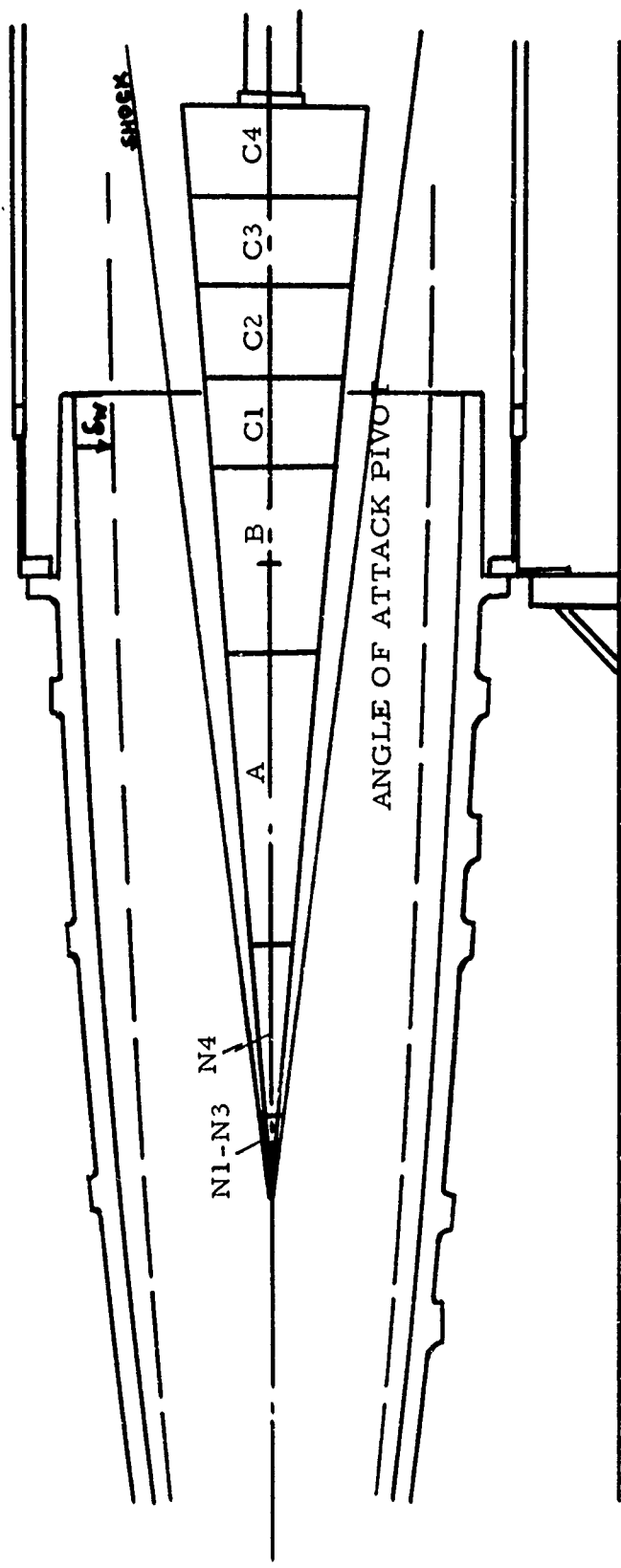


Figure 2  
SKETCH OF 12' CONE MODEL IN NOZZLE.

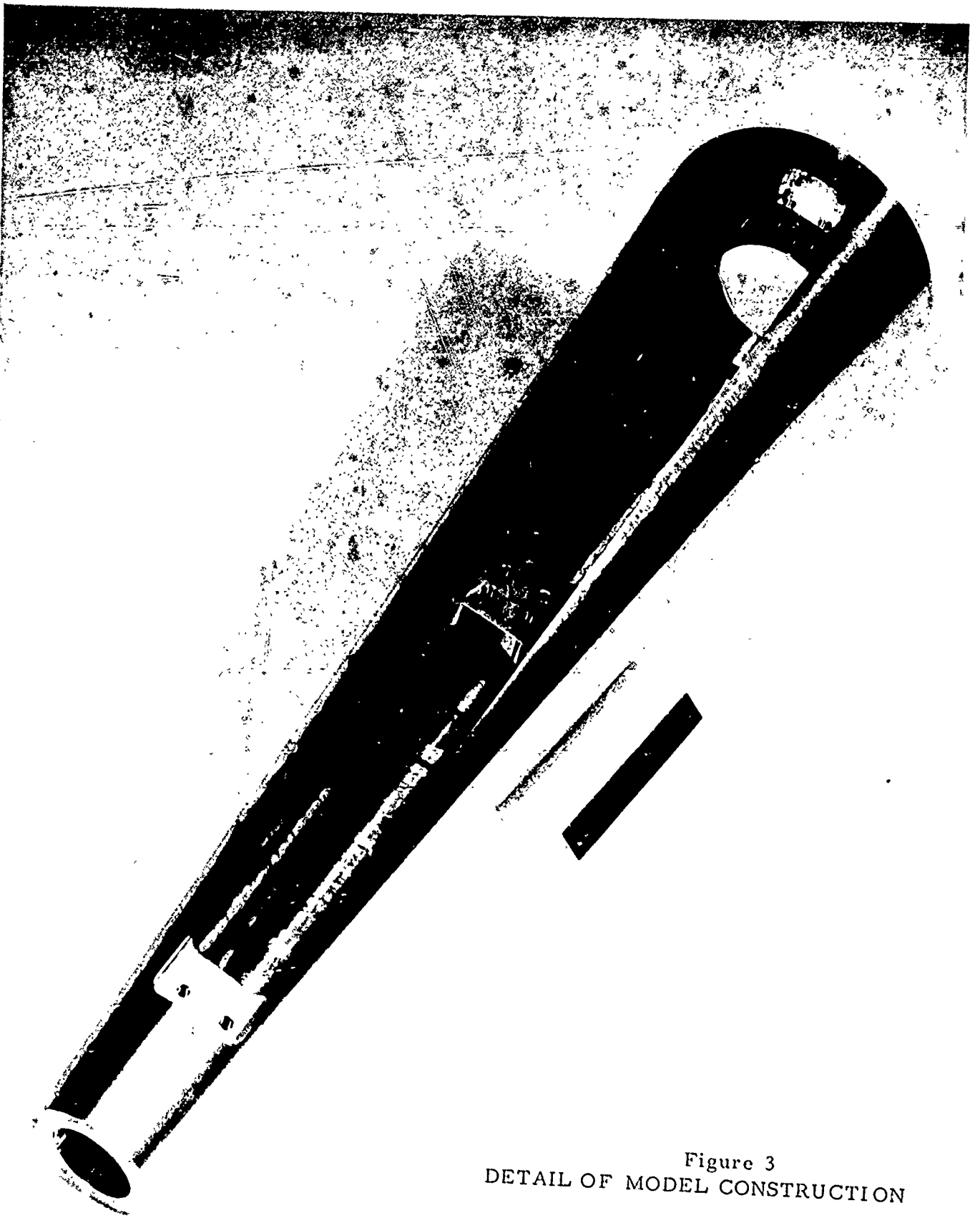


Figure 3  
DETAIL OF MODEL CONSTRUCTION

11/16/68

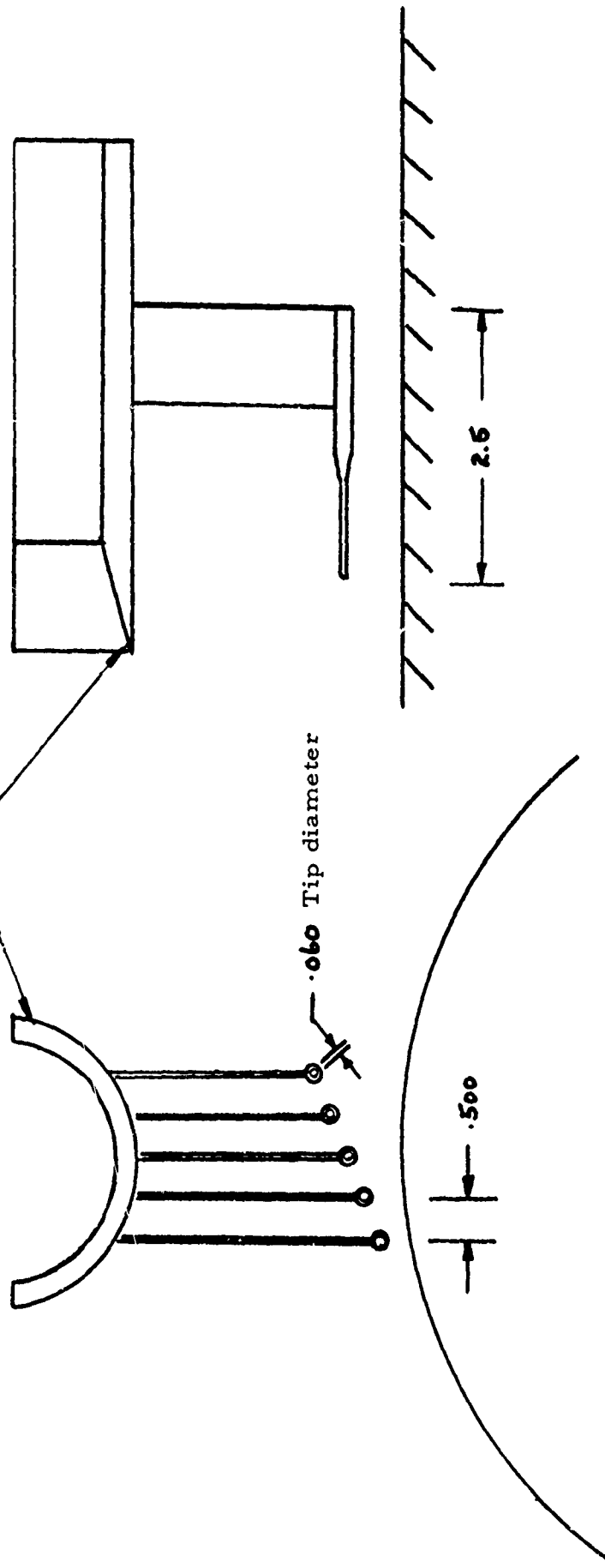


Figure 4  
DETAIL OF SURFACE INSTRUMENTATION



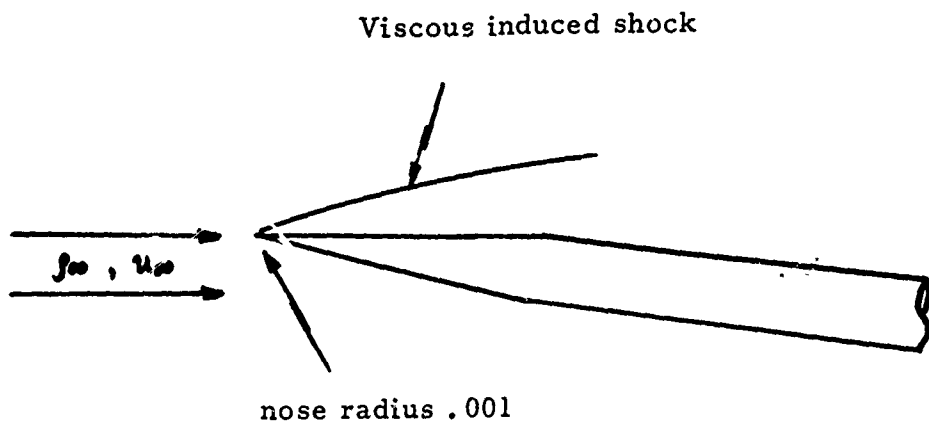
Figure 5  
DETAIL OF PITOT PROBE ASSEMBLY

Assembly is suspended on wires with adjustable angle and position. Hemicylindrical body houses transistor amplifiers.



All dimensions in inches.

Figure 6  
PITOT PROBE LOCATION IN THE BOUNDARY LAYER.



Dimensions in inches

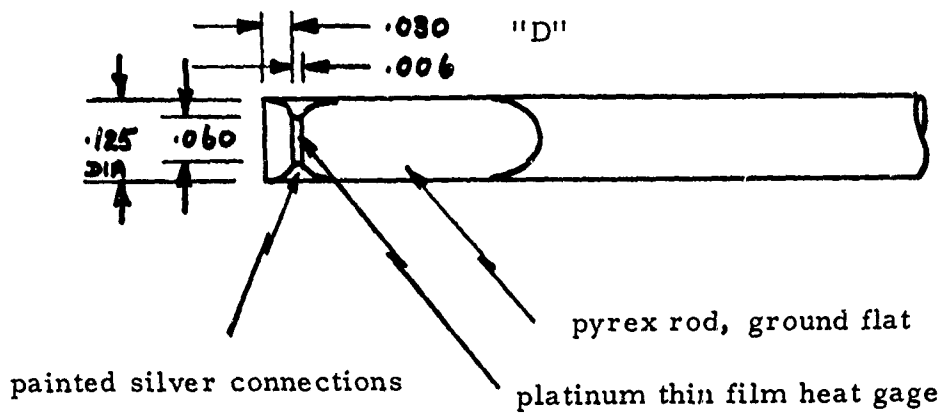
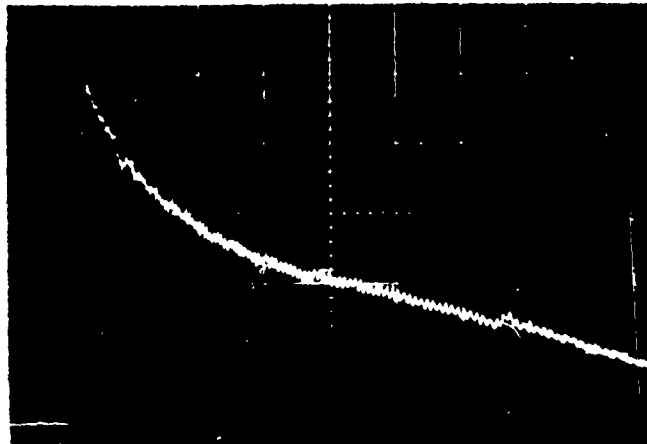
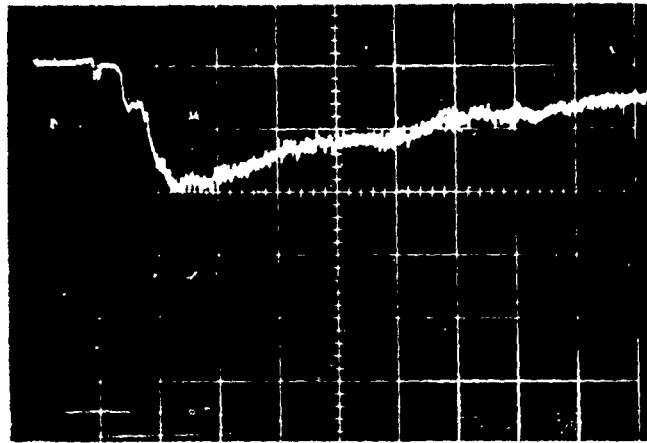


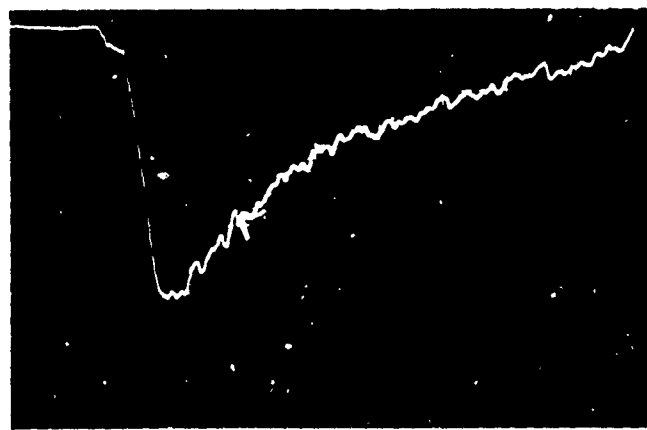
Figure 7  
DETAIL OF WEDGE PROBE.



$P_s$  PLENUM  
PRESSURE



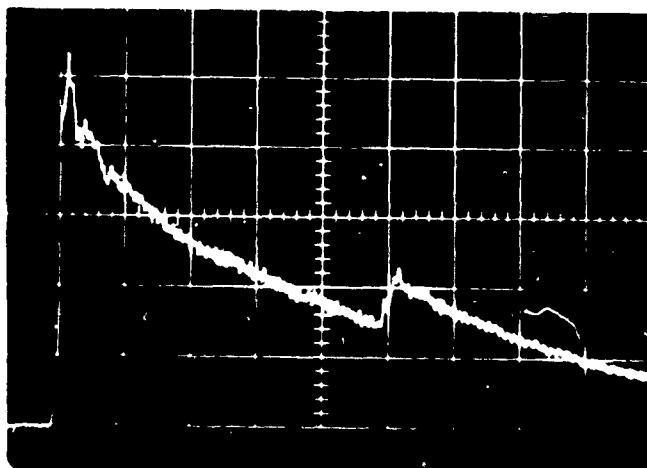
$P_c$  CONE  
PRESSURE



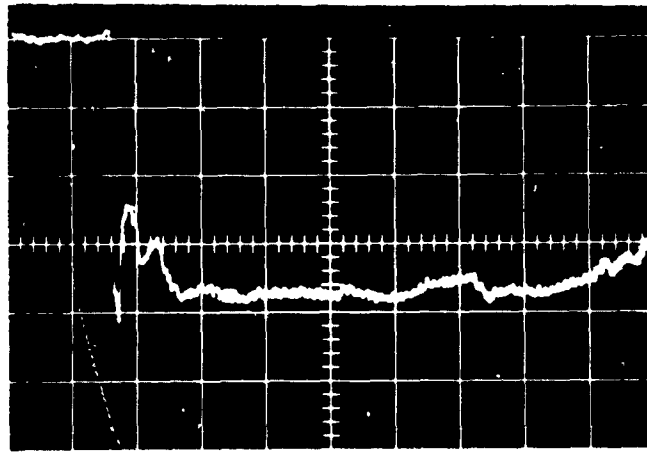
$P'_o$  PITOT  
PRESSURE

→ | ← 2 MILLISEC.

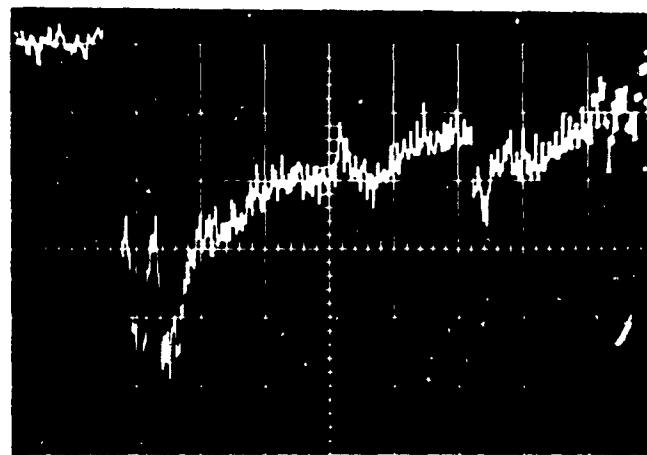
Figure 8  
OSCILLOSCOPE TRACES FOR PRESSURE DATA



↑  $P_s$   
 PLENUM  
 PRESSURE



↓  $T$   
 GAGE SURFACE  
 TEMPERATURE



↓  $q$   
 HEAT TRANSFER  
 (ANALOG OUTPUT)

← 2 MILLISEC. →

Figure 9  
 OSCILLOSCOPE TRACES FOR HEAT TRANSFER DATA

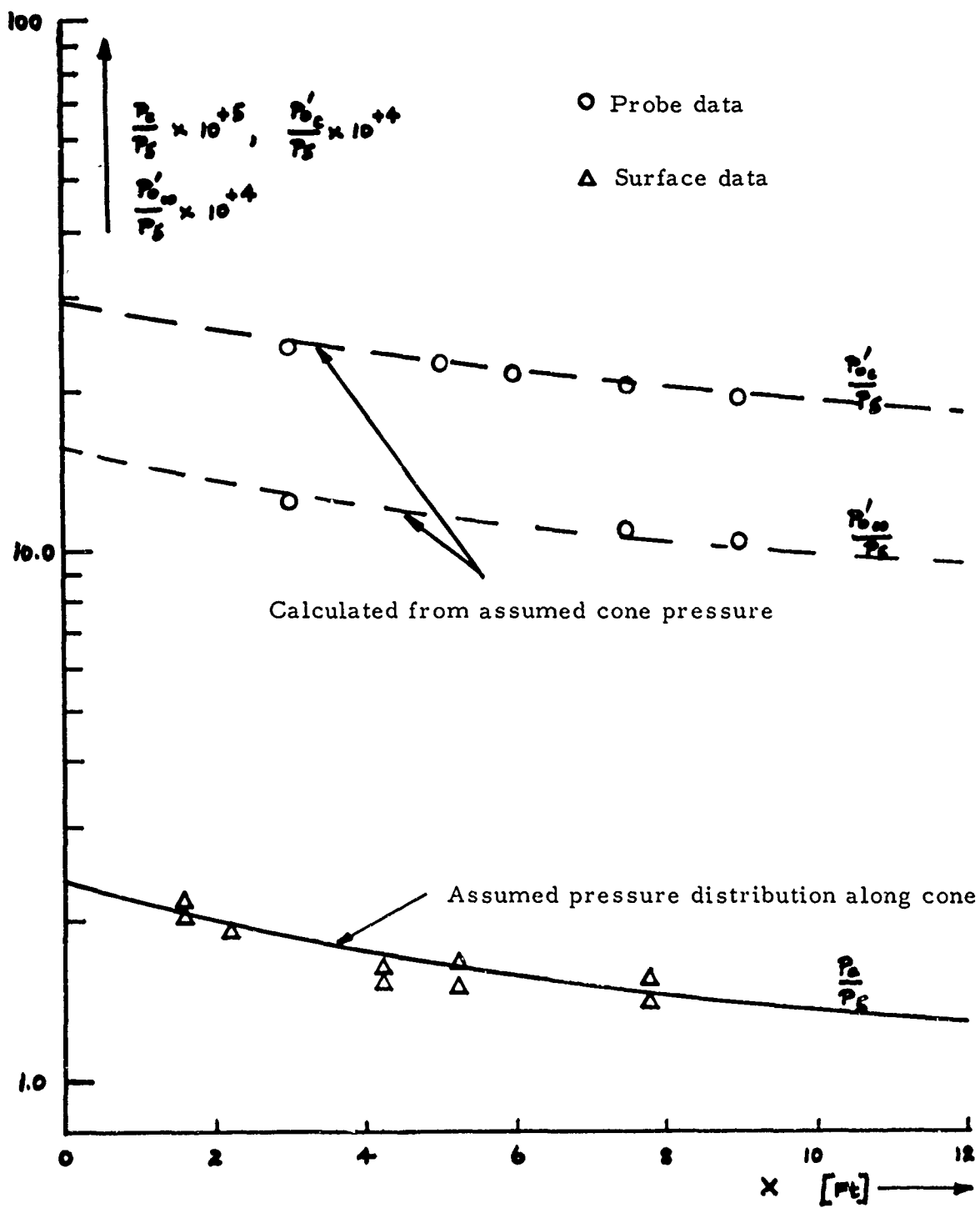


Figure 10  
TYPICAL PRESSURE DISTRIBUTIONS ALONG CONE.

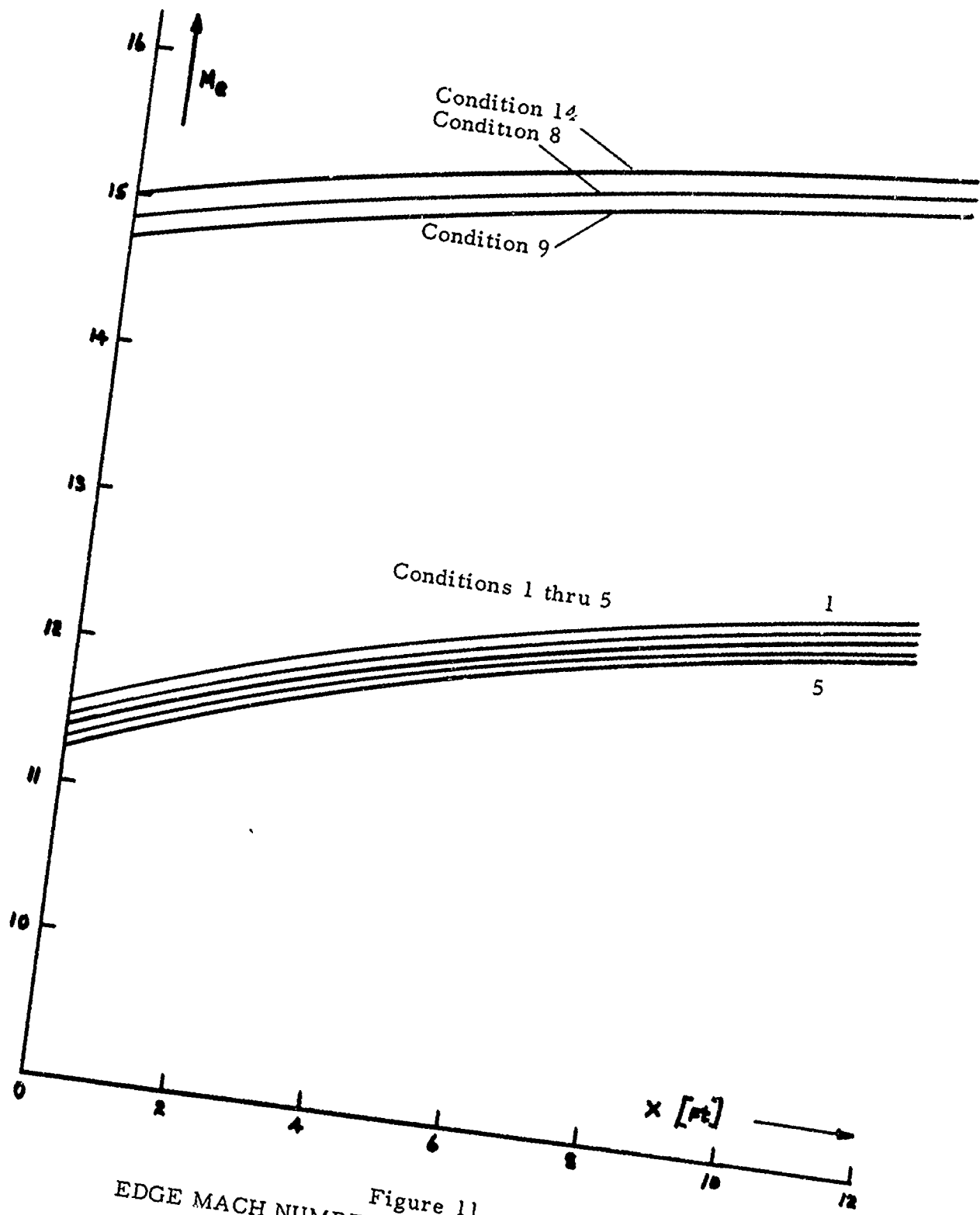


Figure 11  
EDGE MACH NUMBER DISTRIBUTIONS ALONG CONE.

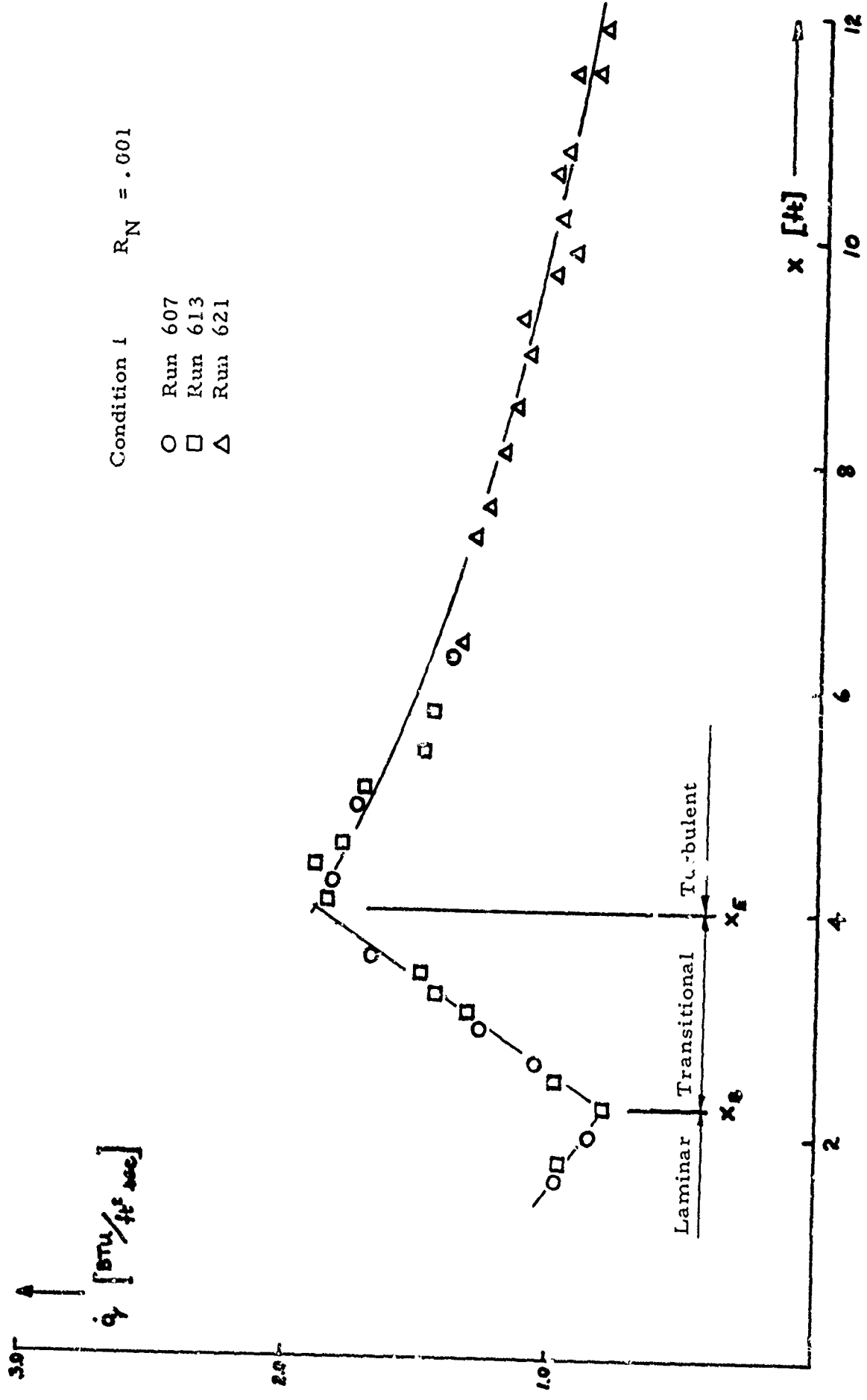


Figure 12  
 TYPICAL HEAT TRANSFER DISTRIBUTION ALONG CONE.

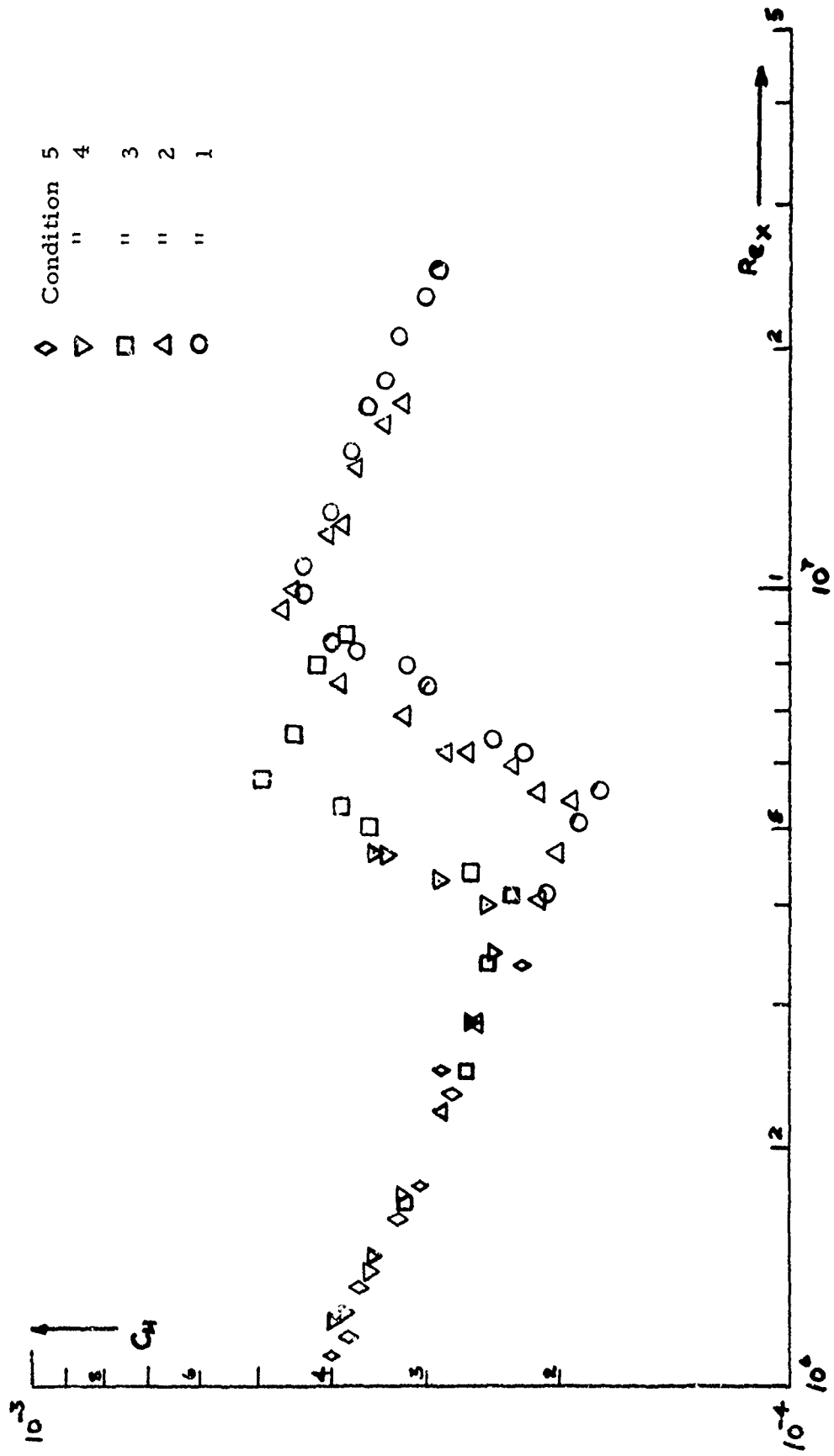


Figure 13  
 NON-DIMENSIONAL HEAT TRANSFER ALONG SHARP CONE.  
 (CONDITIONS 1-5)

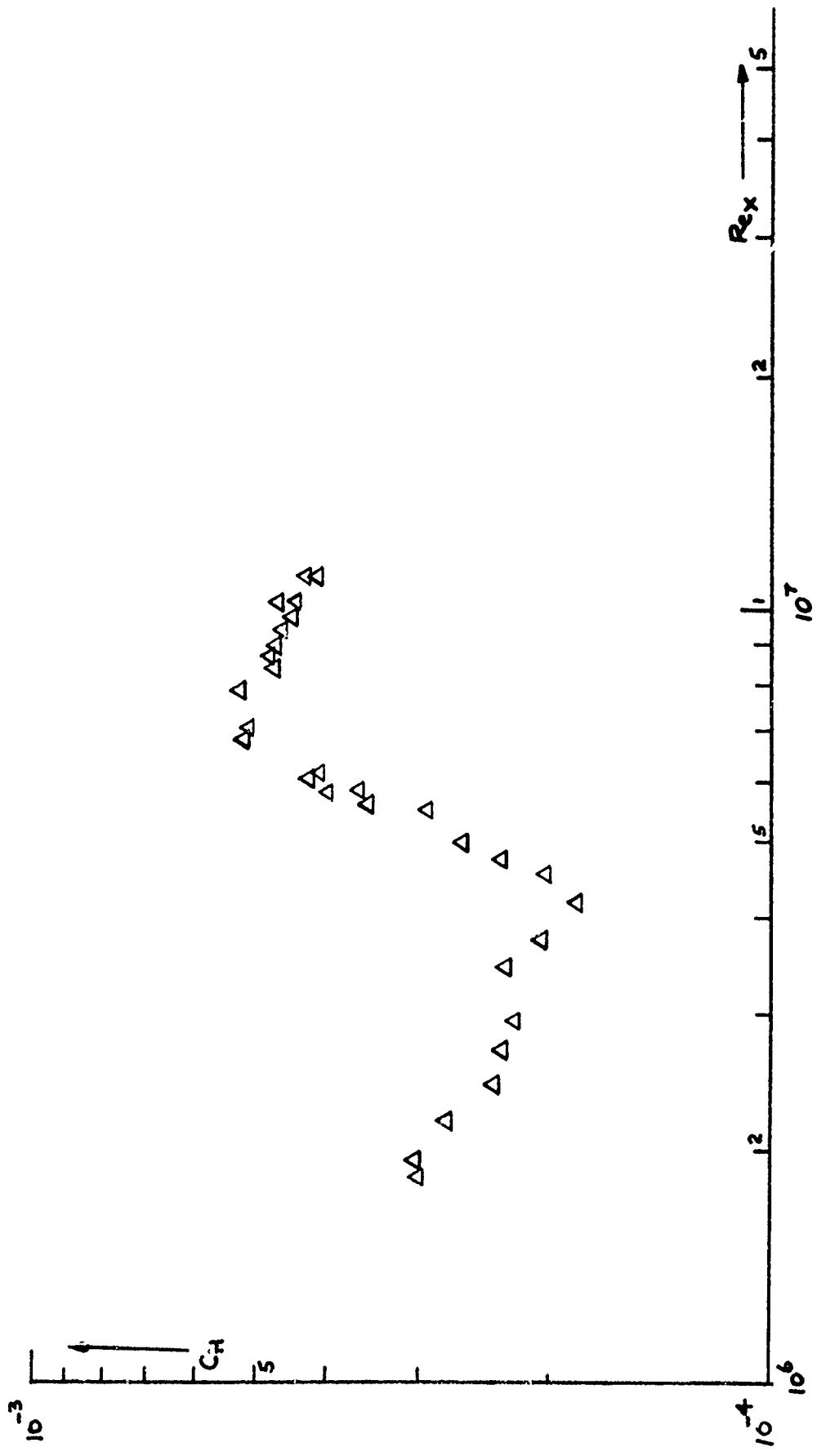


Figure 14.  
 NON-DIMENSIONAL HEAT TRANSFER ALONG SHARP CONE.  
 (CONDITION 6)

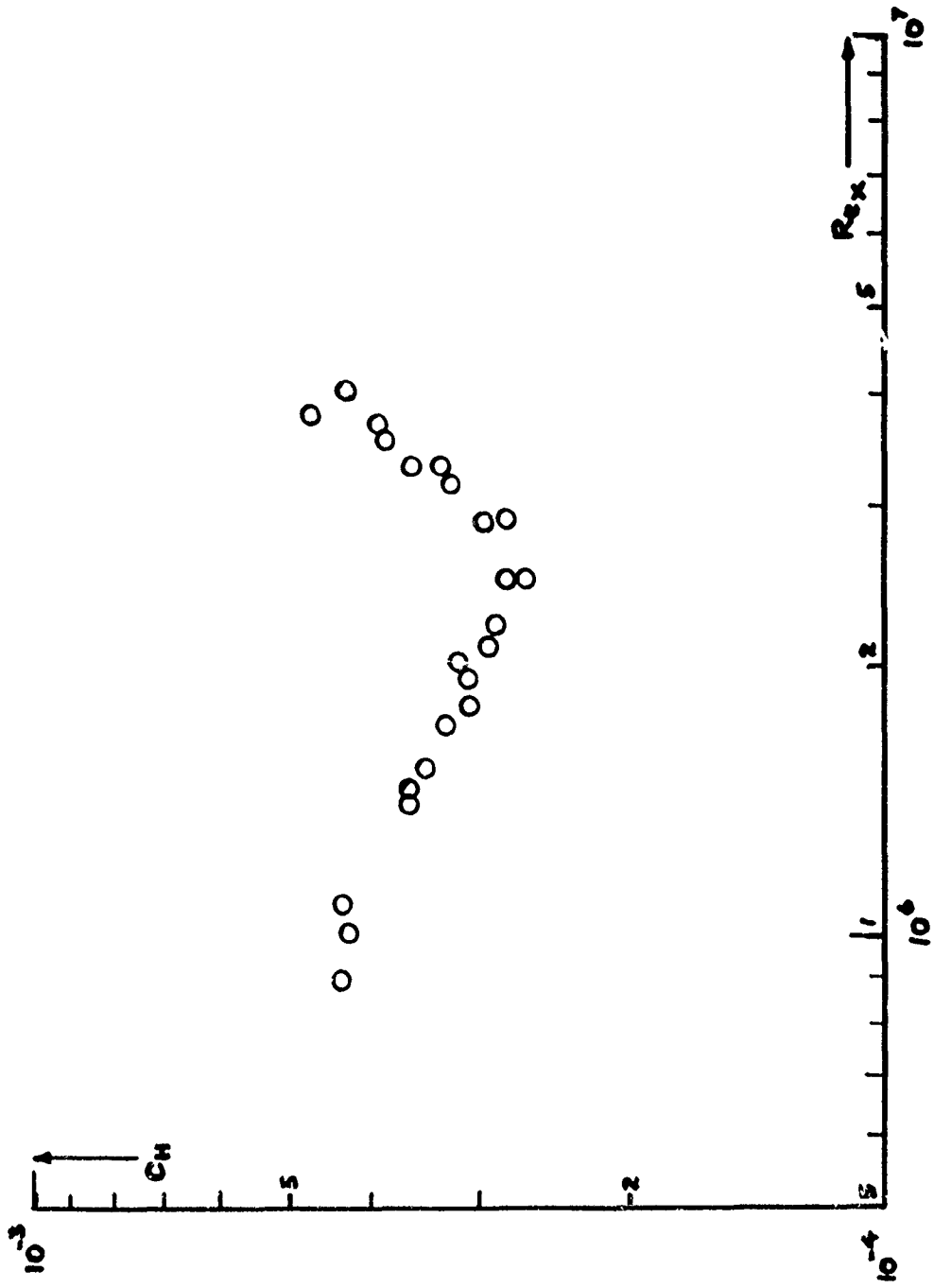


Figure 15  
 NON-DIMENSIONAL HEAT TRANSFER ALONG SHARP CONE.  
 (CONDITION 7).

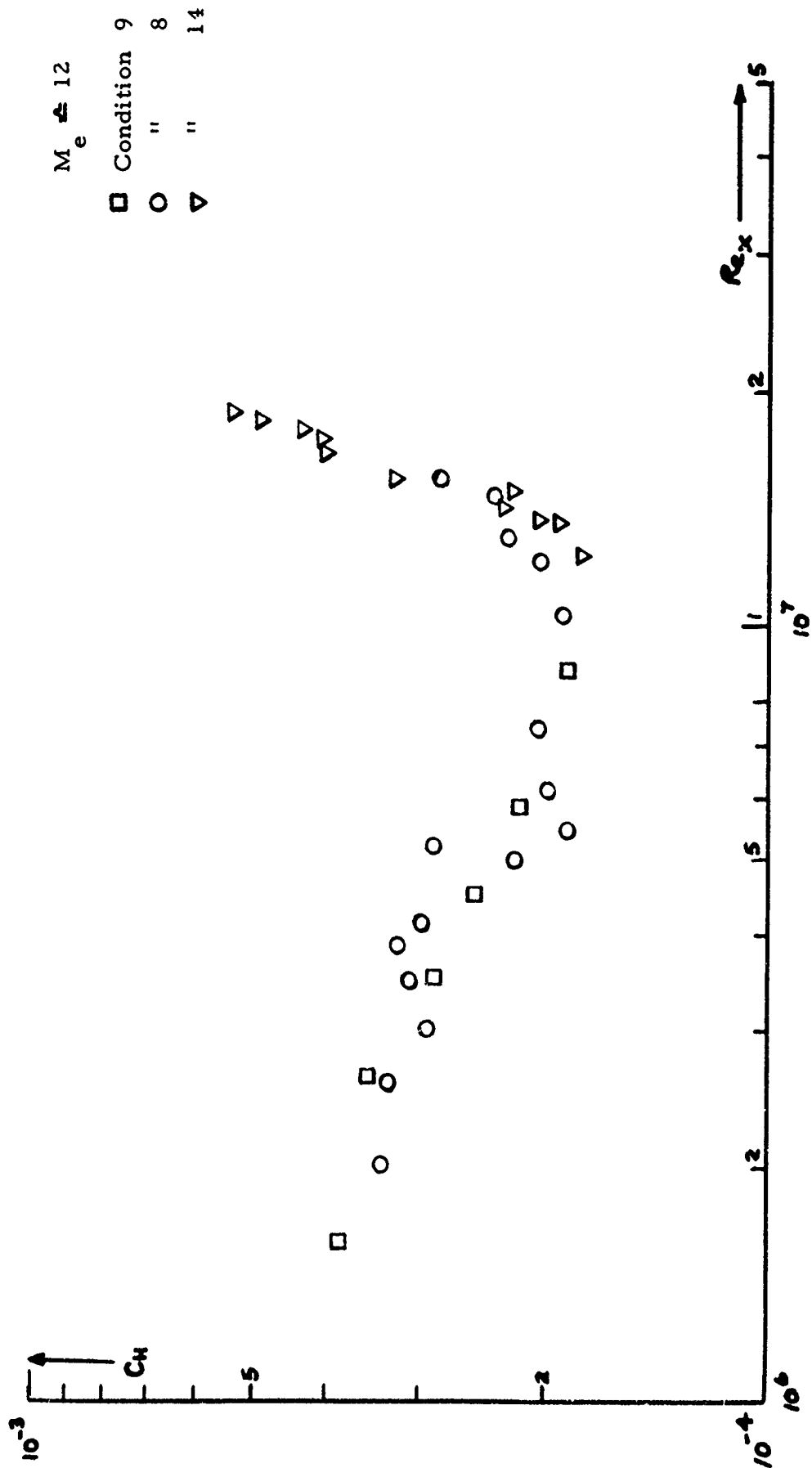


Figure 16  
 NON-DIMENSIONAL HEAT TRANSFER DISTRIBUTION ALONG SHARP CONE.  
 (CONDITIONS 8-9)

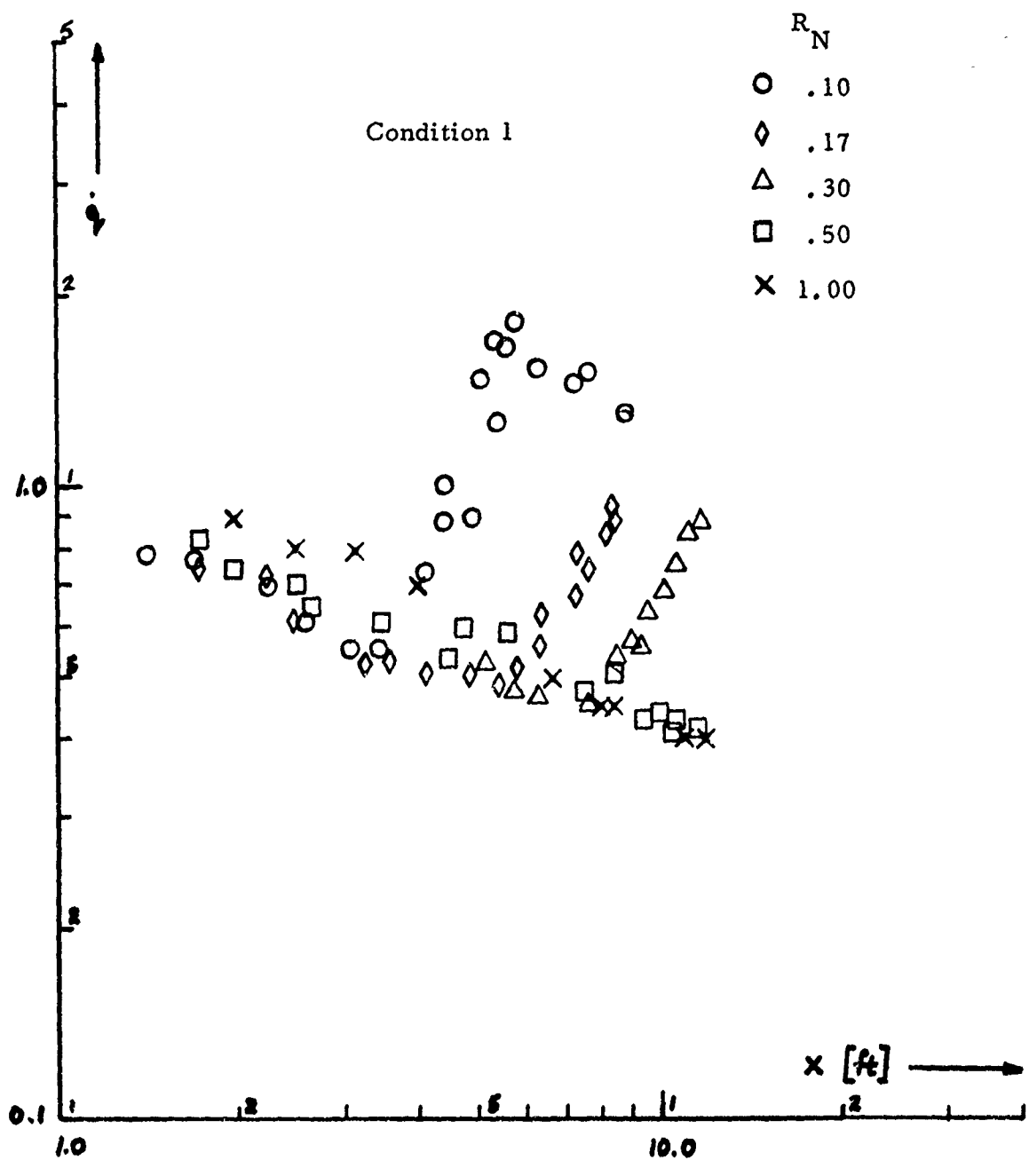


Figure 17  
HEAT TRANSFER DISTRIBUTIONS ALONG BLUNT CONE.

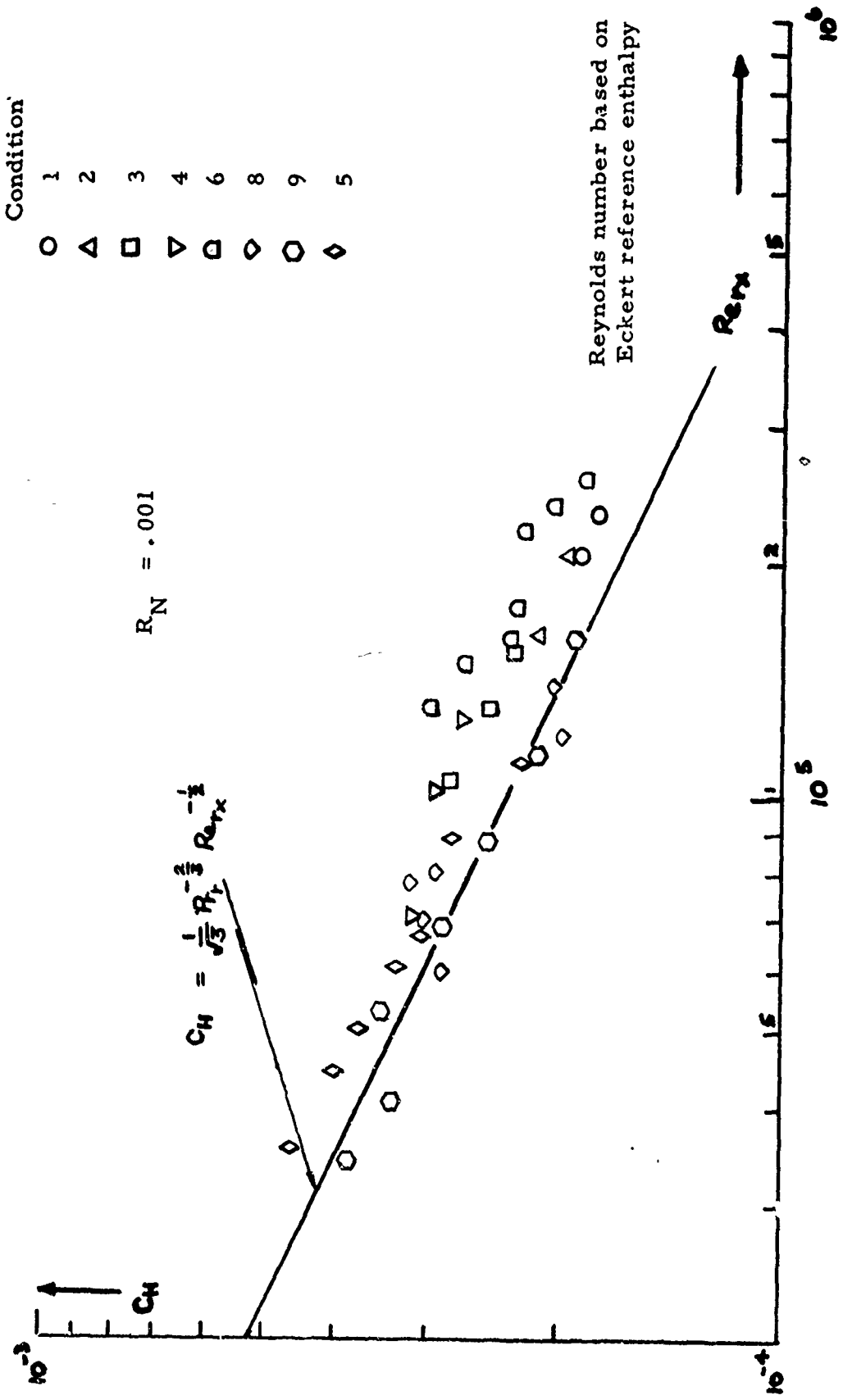


Figure 18  
LAMINAR HEAT TRANSFER CORRELATION.

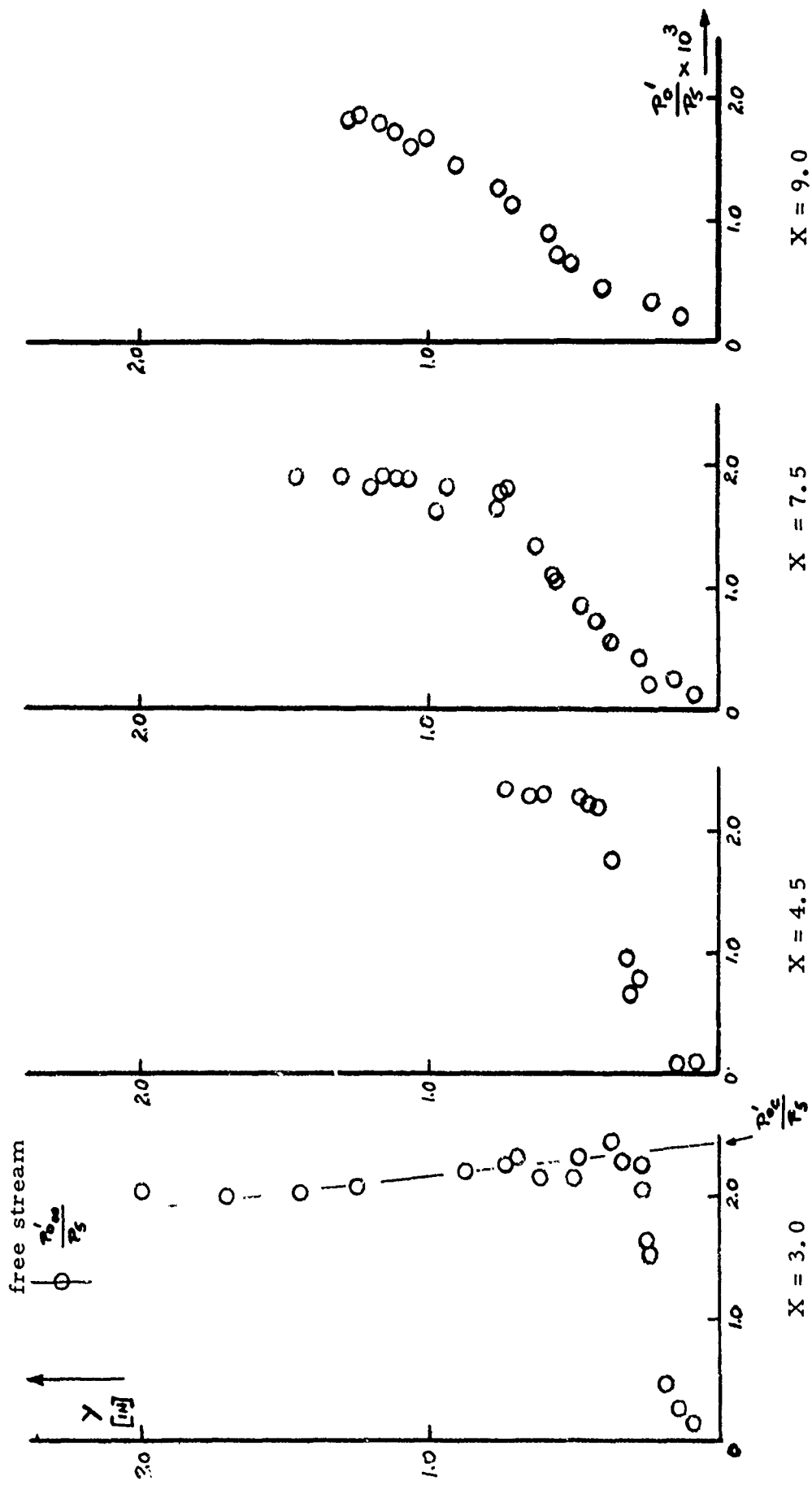


Figure 19  
 PITOT PRESSURE PROFILES ACROSS THE BOUNDARY LAYER.

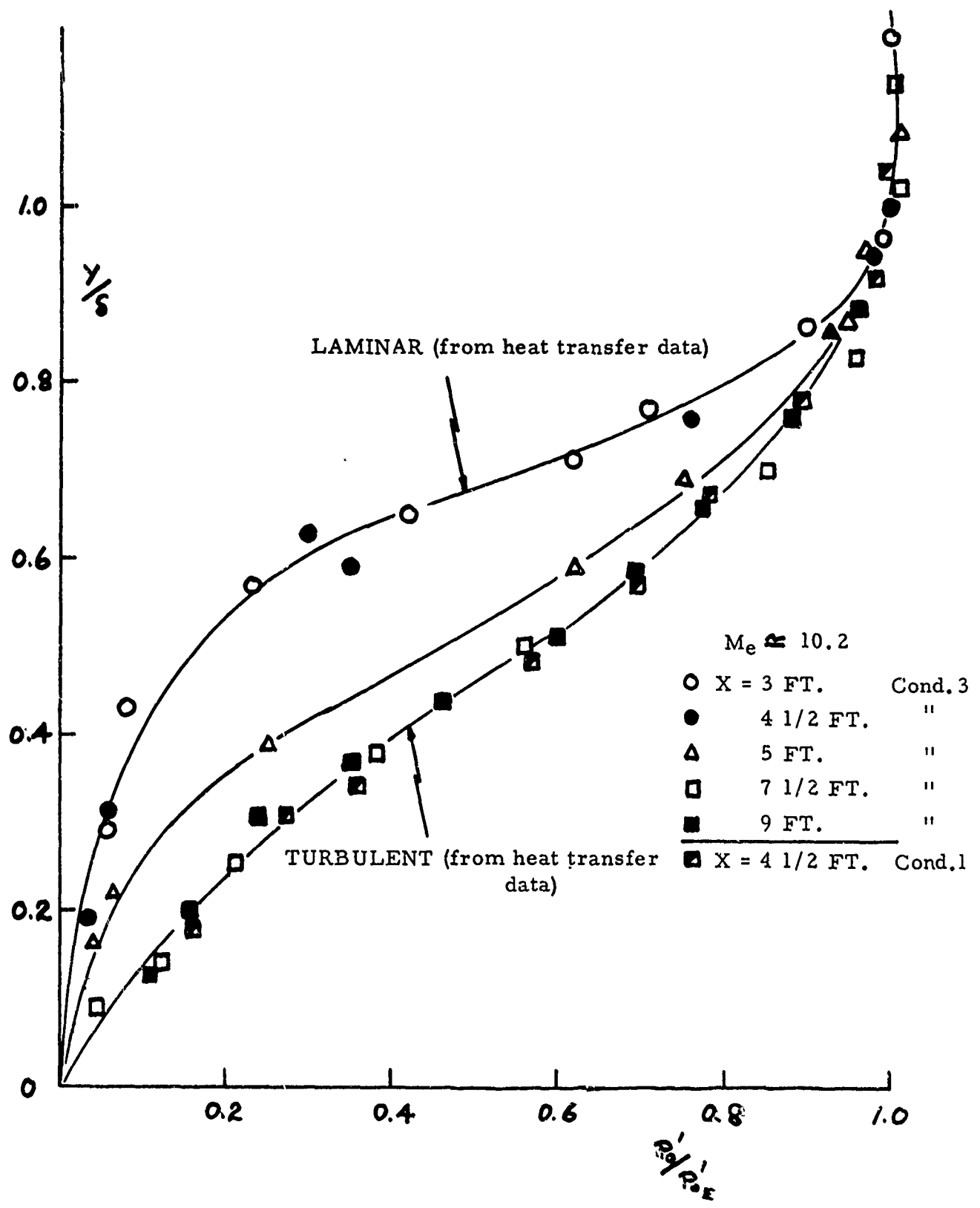


Figure 20  
NON-DIMENSIONAL PITOT PRESSURE PROFILES.

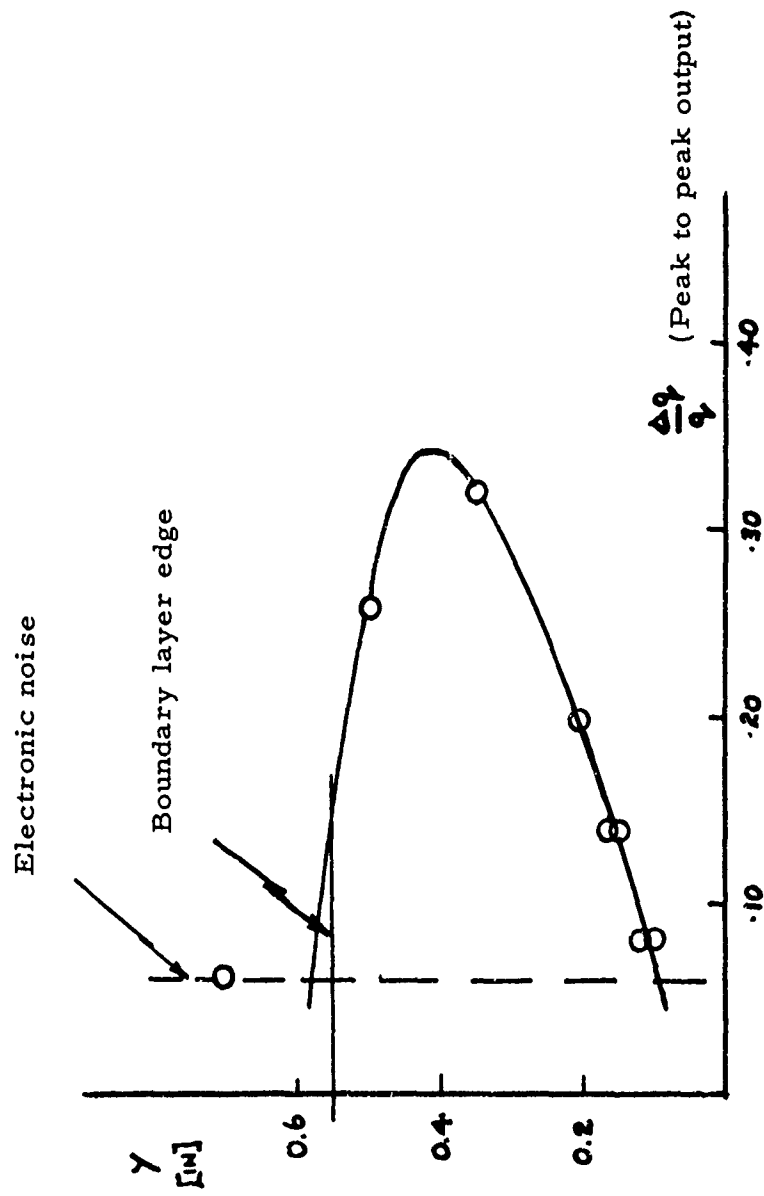


Figure 21  
 WEDGE PROBE FLUCTUATIONS ACROSS LAMINAR BOUNDARY LAYER AT  $X_B$

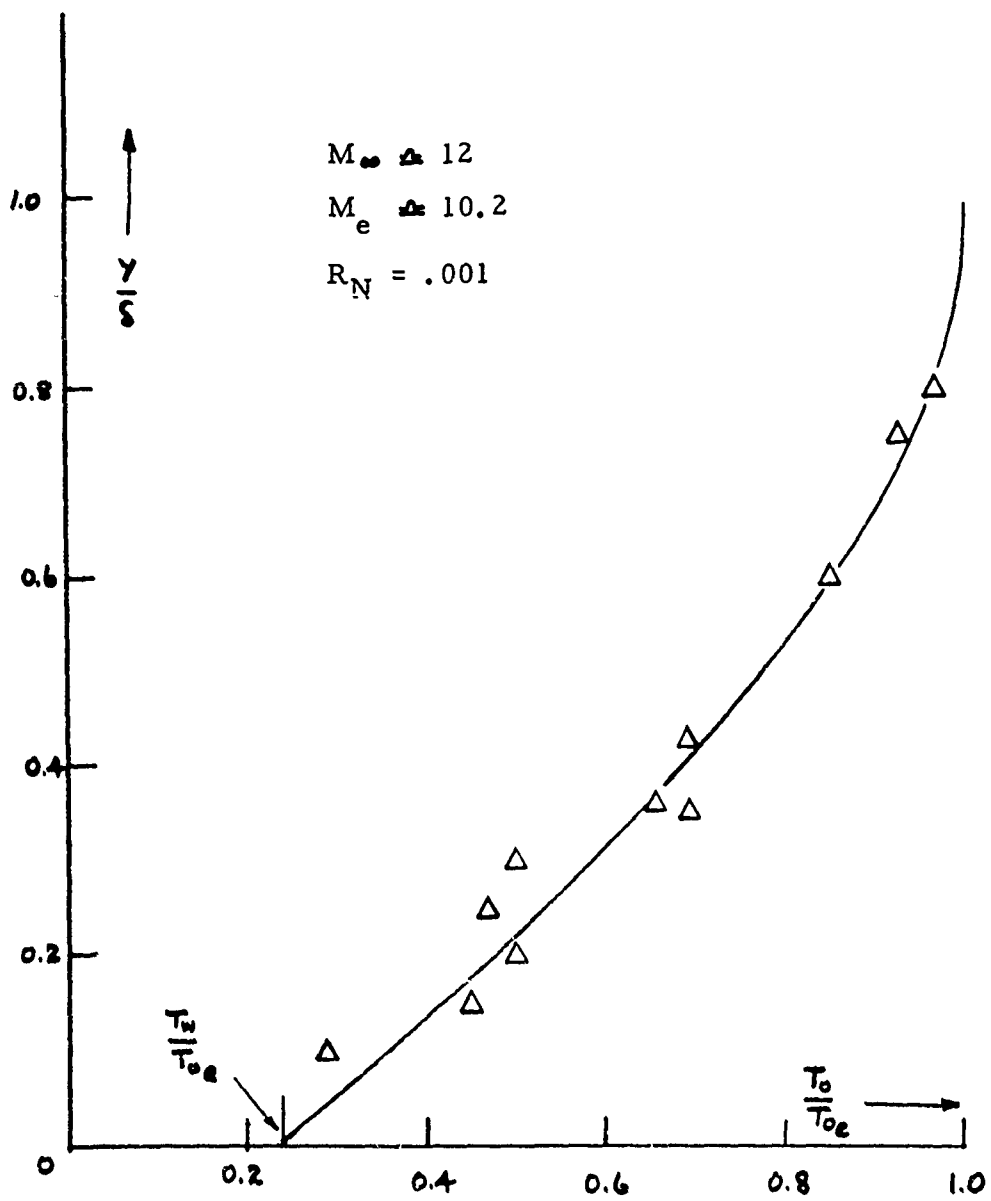


Figure 22  
TOTAL TEMPERATURE ACROSS LAMINAR BOUNDARY LAYER.

$$M_\infty \approx 12$$

$$M_e \approx 10.2$$

$$R_N = .001$$

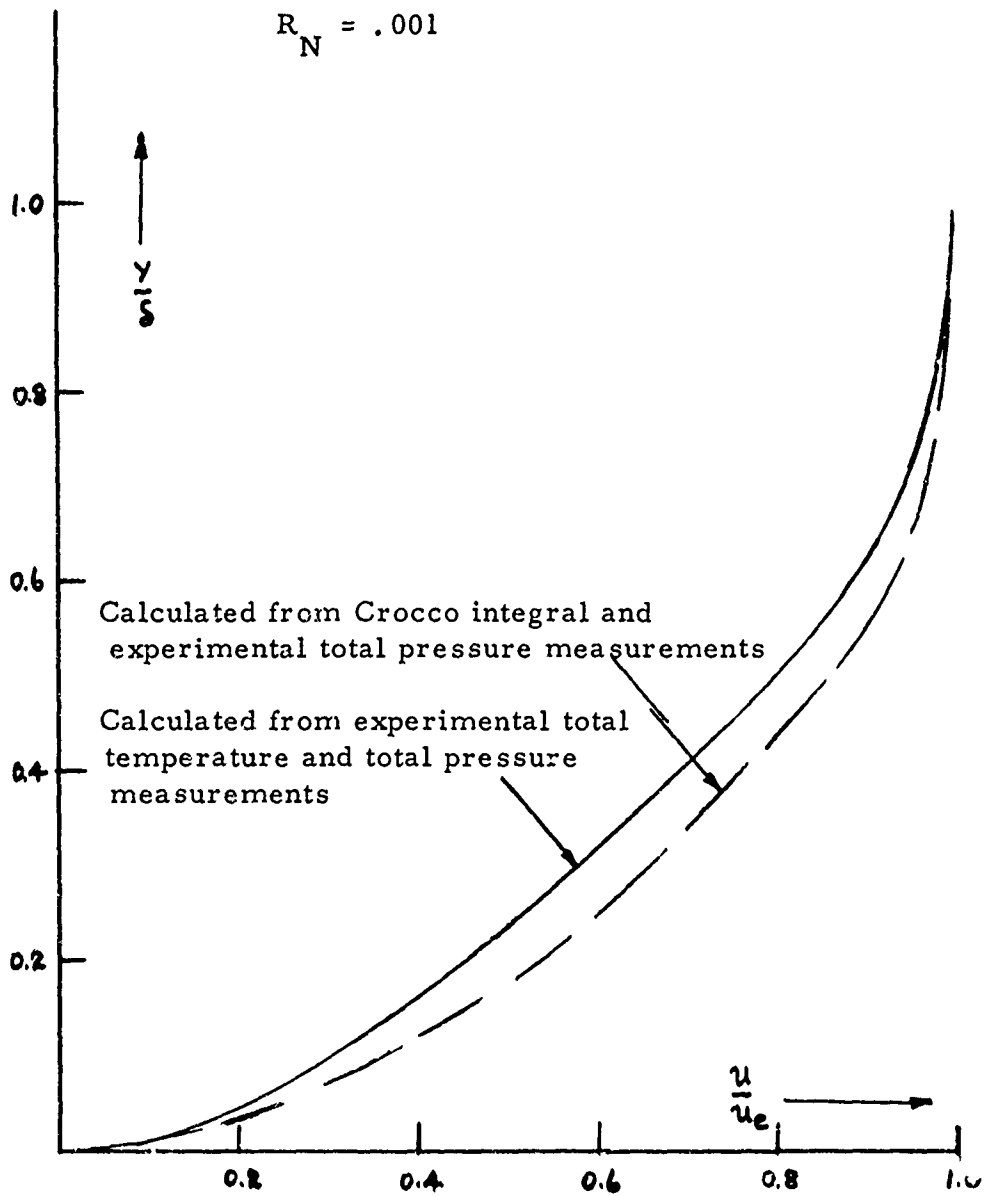
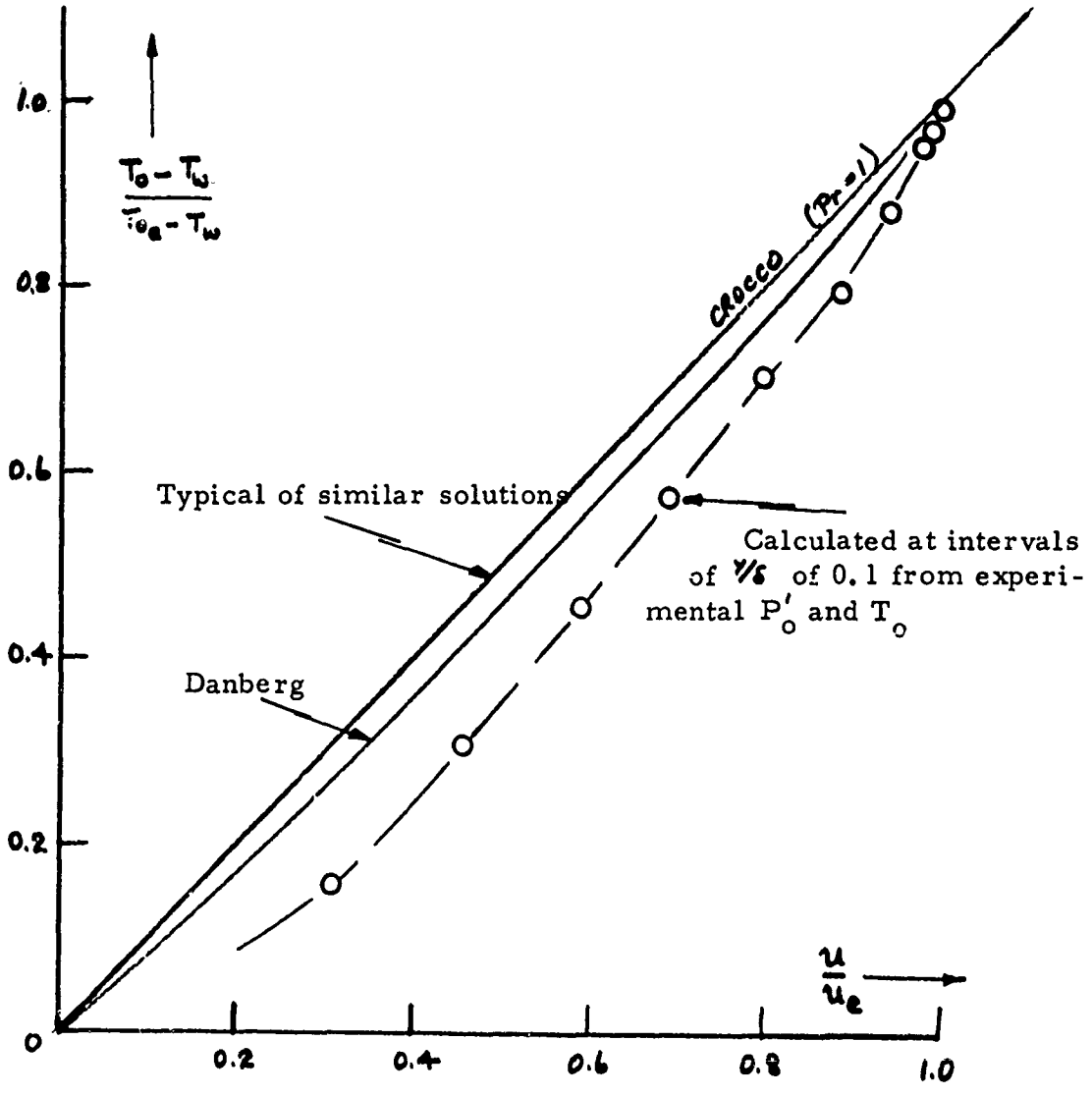


Figure 23  
VELOCITY DISTRIBUTION ACROSS LAMINAR BOUNDARY LAYER.

Figure 24  
 TOTAL TEMPERATURE AS A FUNCTION OF VELOCITY ACROSS  
 LAMINAR BOUNDARY LAYER

$M_\infty \approx 12$   
 $M_e \approx 10.2$   
 $R_N = .001$   
 $T_w/T_R = .26$



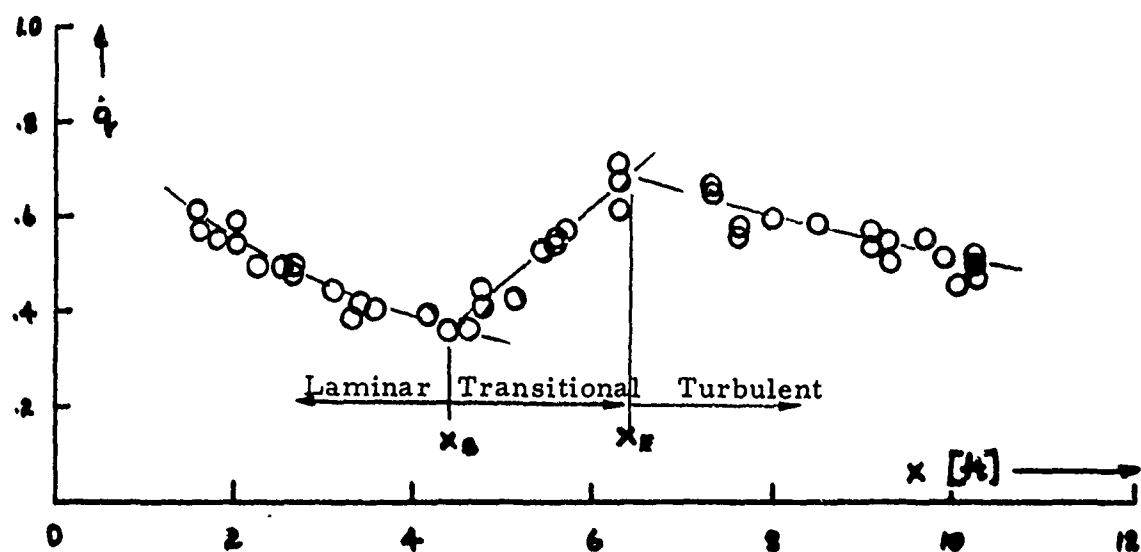
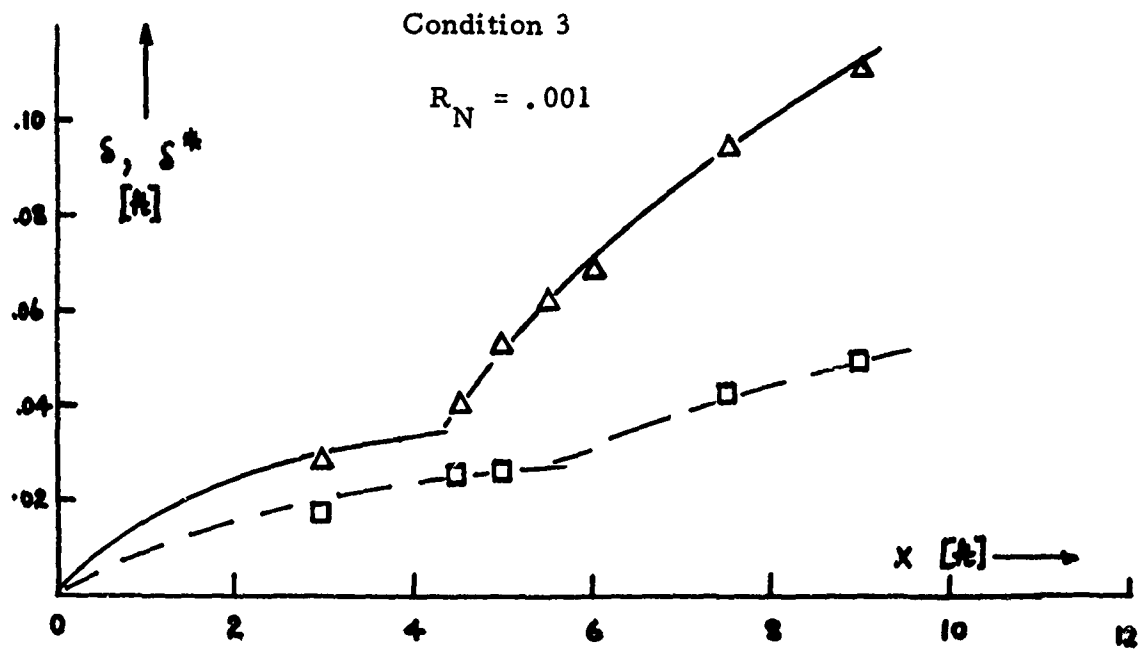


Figure 25  
 BOUNDARY LAYER THICKNESS GROWTH COMPARED WITH  
 HEAT TRANSFER DISTRIBUTION.

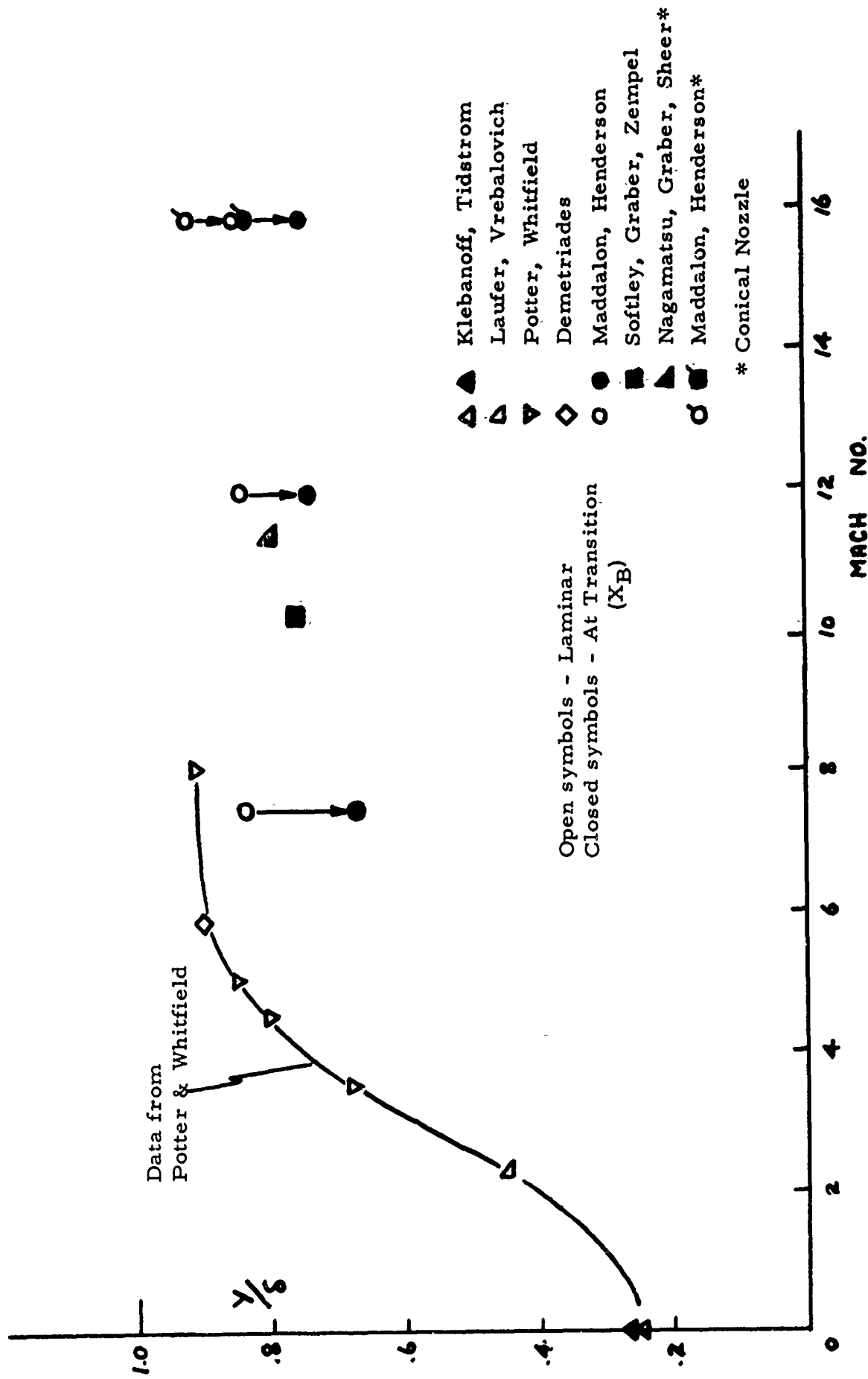


Figure 26  
 EXPERIMENTAL OBSERVATIONS OF LOCATION OF MAXIMUM DISTURBANCES

$T_w/T_R$	$M_e$
○ .26	10.1 - 10.5
◇ .21	10.1 - 10.4
▲ .16	10.0
□ .12	9.7
▼ .25	12.2 - 12.4
▲ .21	12.2

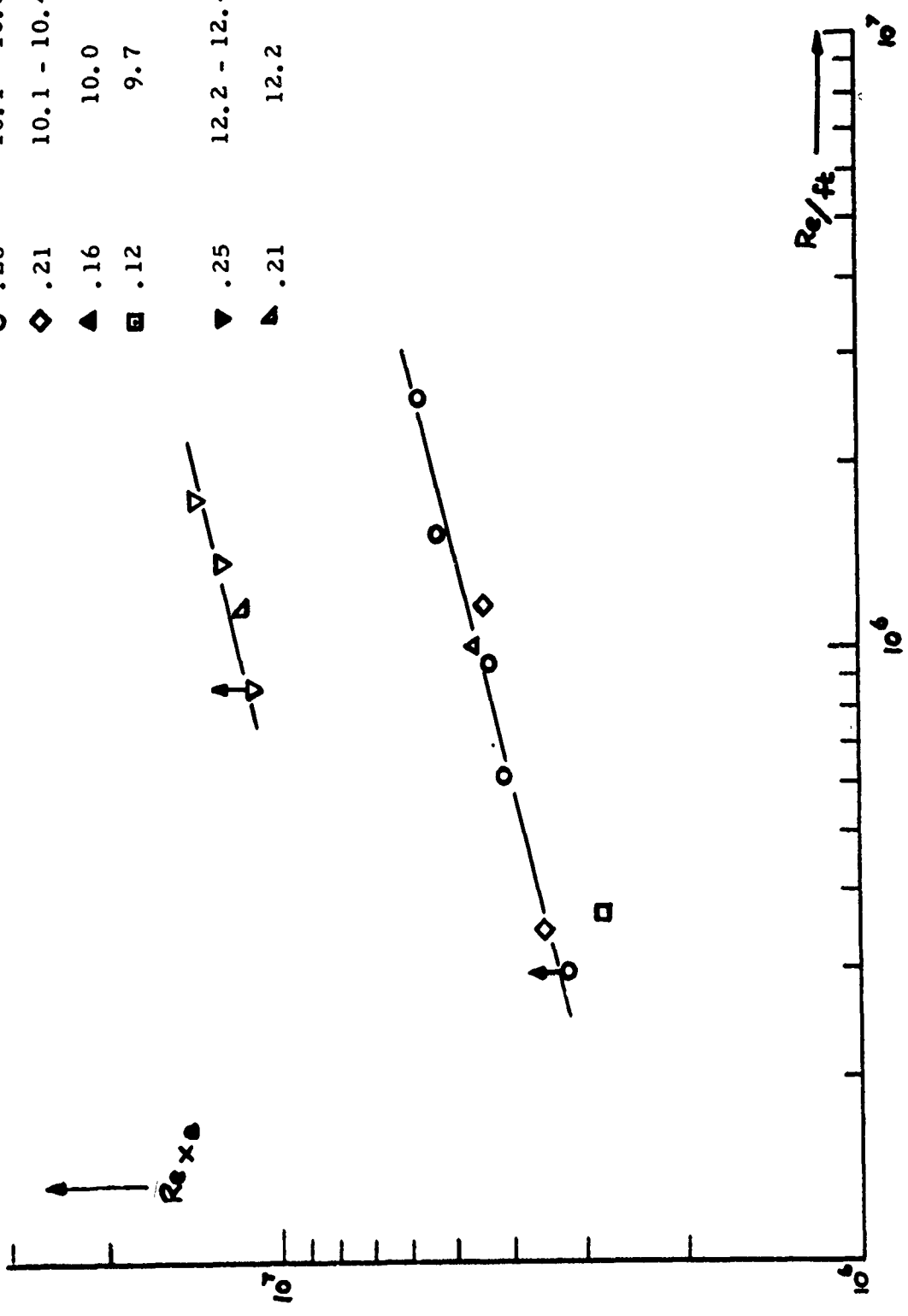


Figure 27  
 TRANSITION REYNOLDS NUMBER AS A FUNCTION OF UNIT REYNOLDS NUMBER.

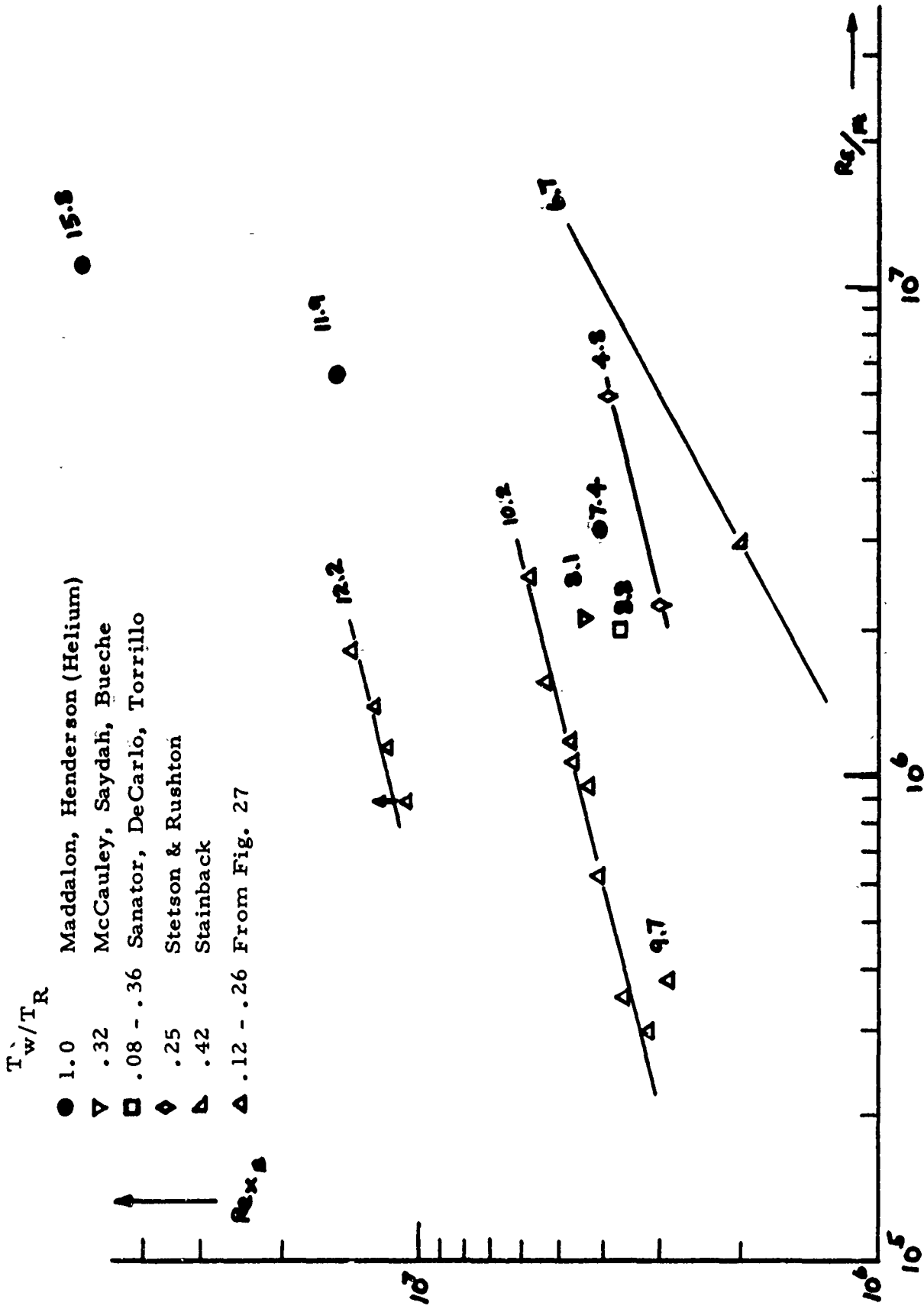


Figure 28  
 COMPARISON OF TRANSITION REYNOLDS NUMBERS WITH RESULTS FROM OTHER FACILITIES.  
 Sharp Slender Cone - Uniform Wall Temperature

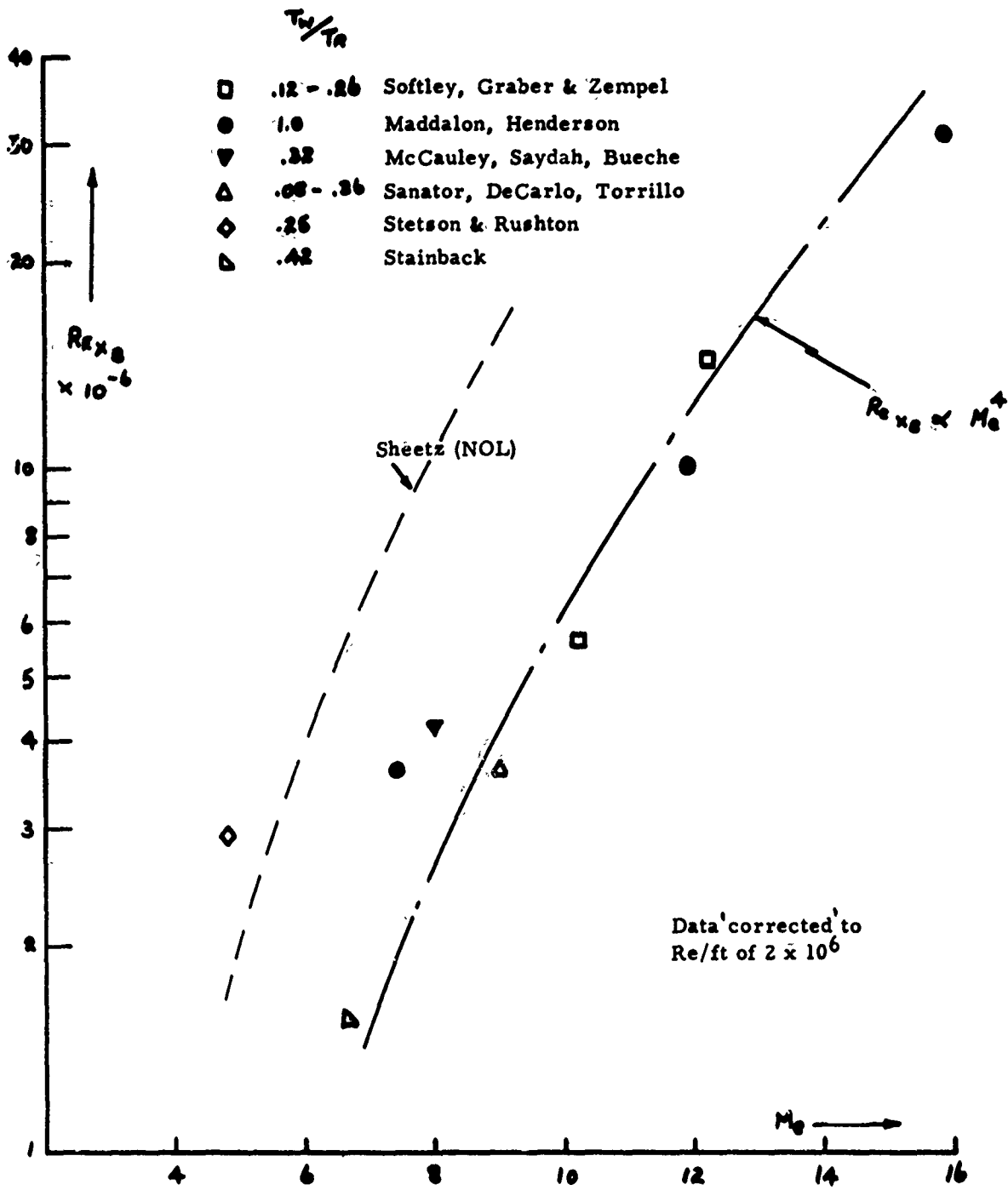
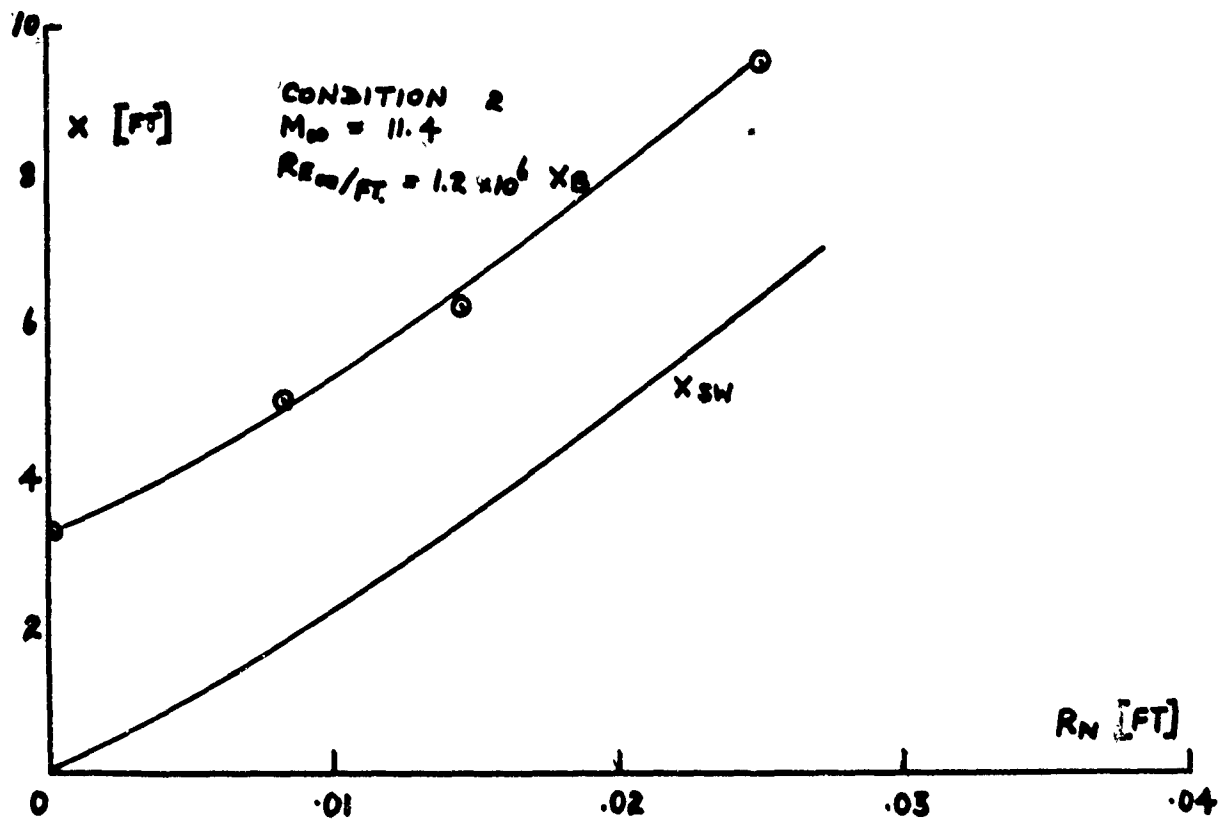
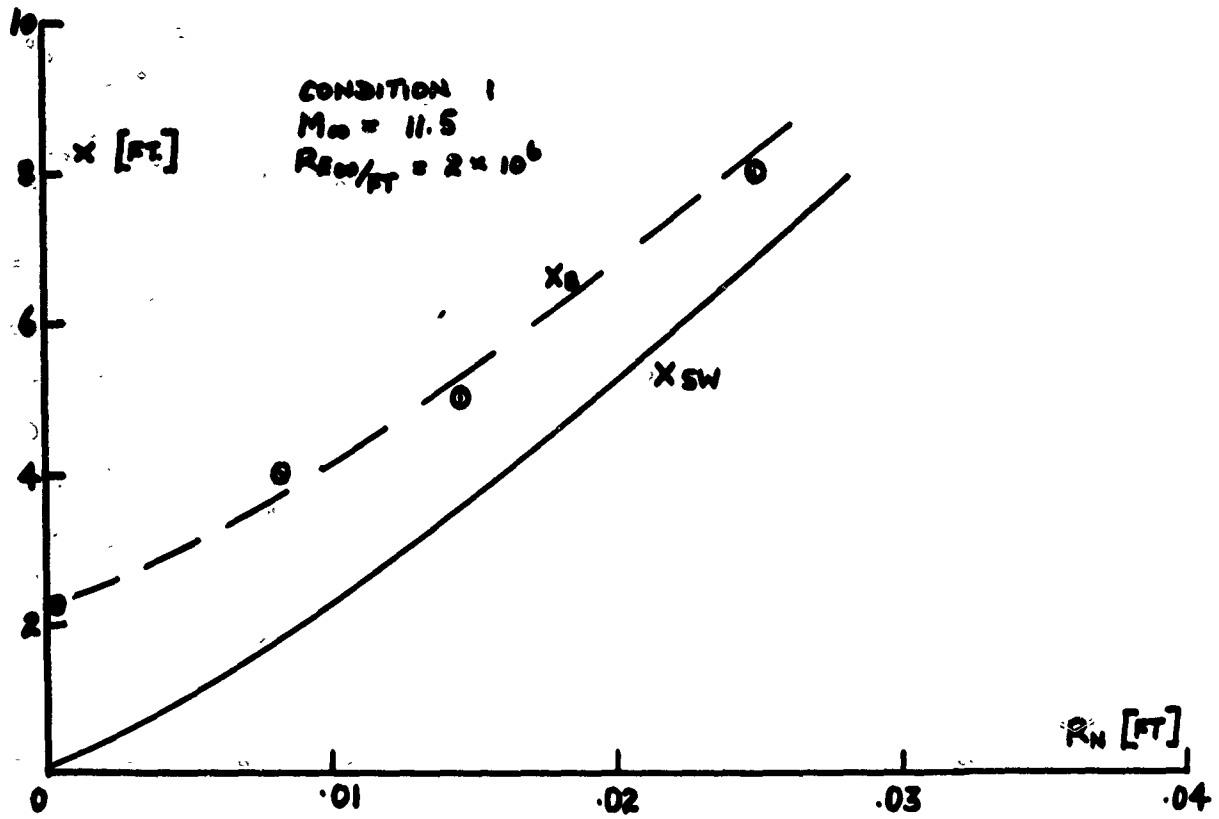


Figure 29  
EFFECT OF LOCAL MACH NUMBER ON TRANSITION REYNOLDS NUMBER  
Sharp Slender Cone - Uniform Wall Temperature

Figure 30  
 MOVEMENT OF TRANSITION LOCATION WITH INCREASING NOSE RADIUS.



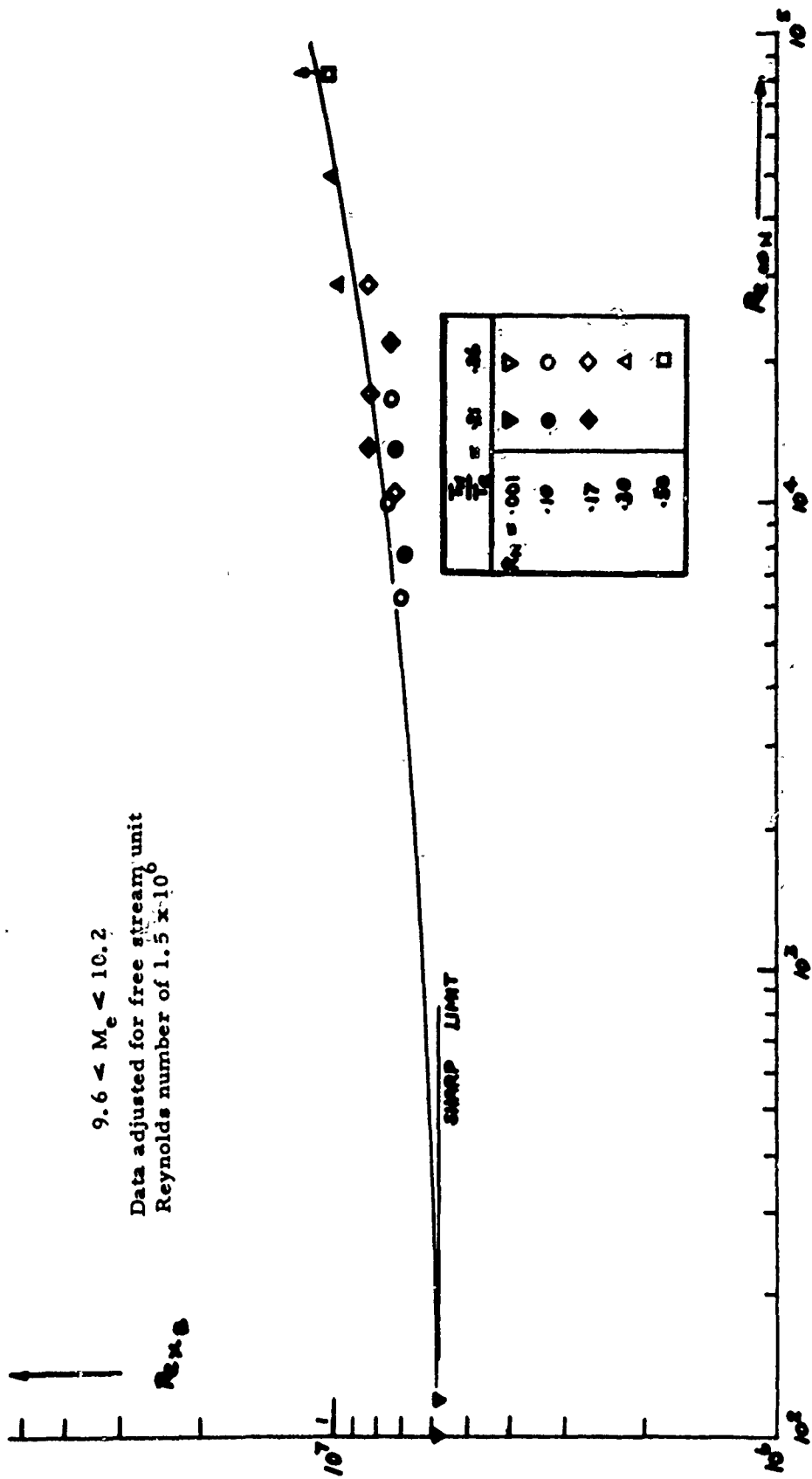


Figure 31  
 TRANSITION REYNOLDS NUMBER AS A FUNCTION OF NOSE REYNOLDS NUMBER.

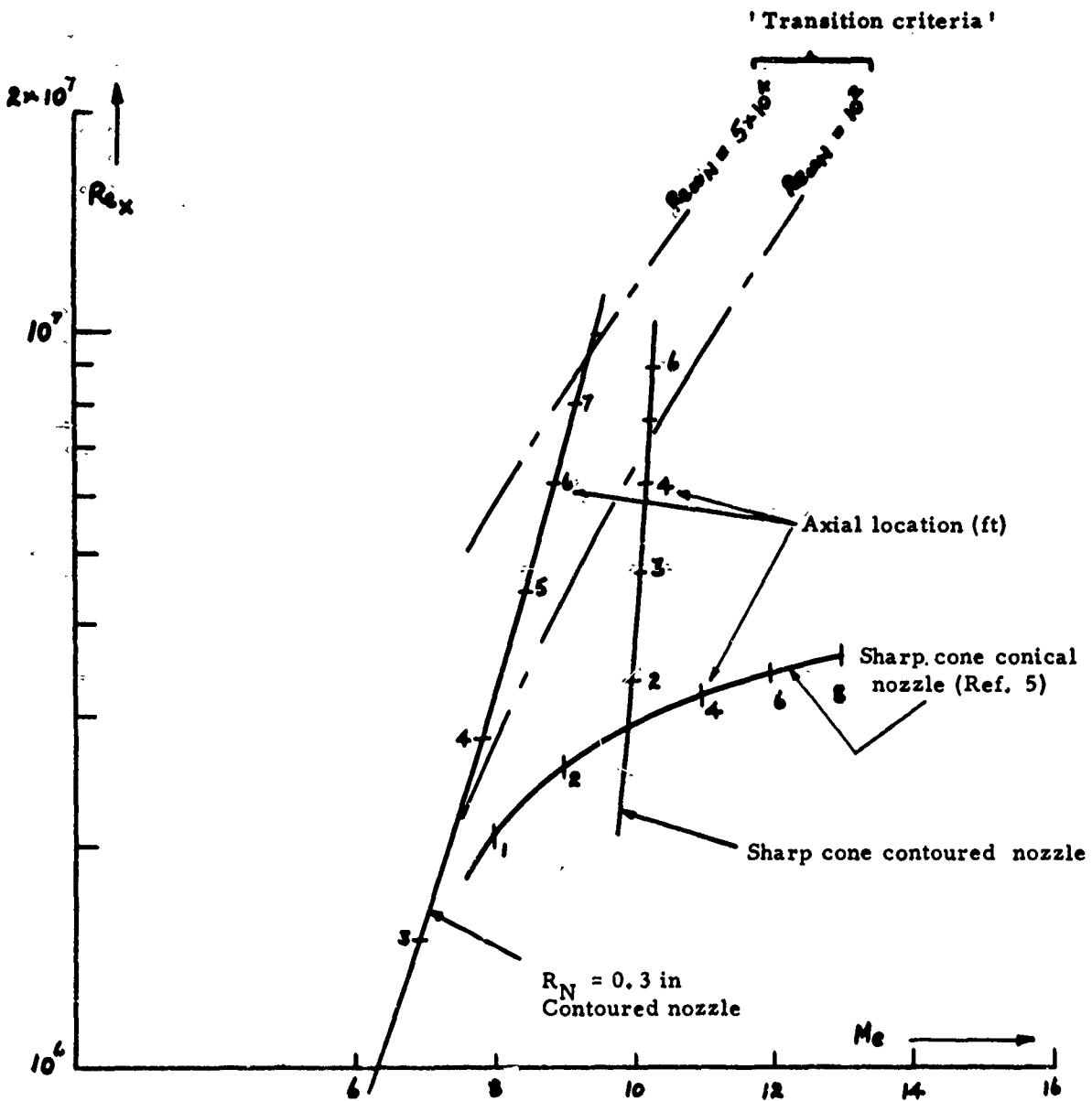


Figure 32  
 REYNOLDS NUMBER, MACH NUMBER HISTORIES FOR THREE MODEL  
 NOZZLE CONFIGURATIONS.

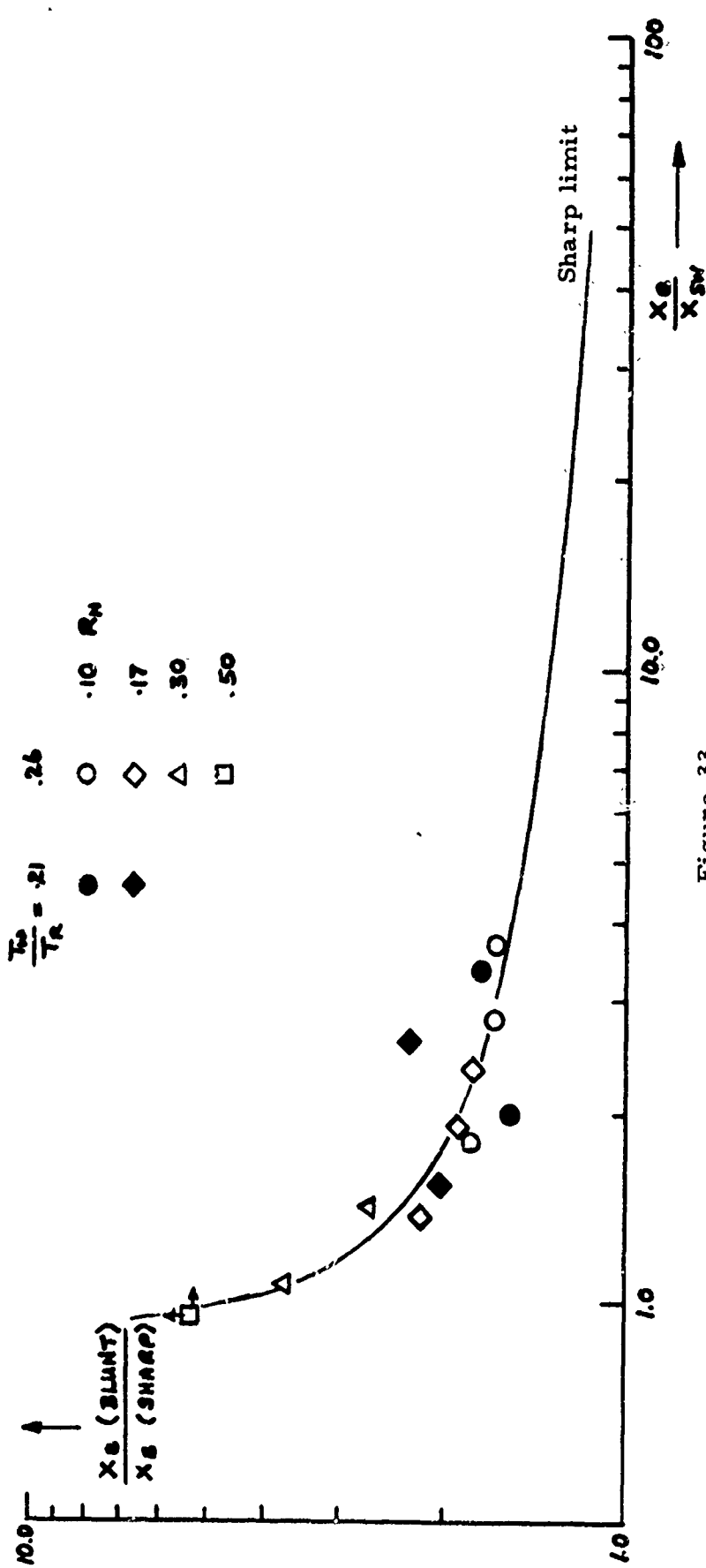


Figure 33  
TRANSITION LOCATION WITH RESPECT TO SWALLOWING DISTANCES.

SPACE SCIENCES LABORATORY  
MISSILE AND SPACE DIVISION

GENERAL ELECTRIC

TECHNICAL INFORMATION SERIES

<b>AUTHOR</b> E. J. Softley B. C. Graber R. E. Zempel	<b>SUBJECT CLASSIFICATION</b> Experimental Fluid Physics	<b>NO.</b> R67SD39
		<b>DATE</b> Dec. 1967
<b>TITLE</b> Transition of the Hypersonic Boundary Layer on a Cone: Part I - Experiments at $M_{\infty} = 12$ and 15.		<b>G. E. CLASS</b> I
		<b>GOV. CLASS</b> Unclassified
<b>REPRODUCIBLE COPY FILED AT MSD LIBRARY. DOCUMENTS LIBRARY UNIT. VALLEY FORGE SPACE TECHNOLOGY CENTER, KING OF PRUSSIA, PA.</b>		<b>NO. PAGES</b> 57
<b>SUMMARY</b> The GE-SSL shock tunnel, fitted with a large contoured nozzle, has been used to observe transition of the boundary layer on a 12 ft., $5^{\circ}$ cone. Free stream flow Mach numbers were 12 and 15 and were essentially uniform. Surface heat transfer distributions were obtained and these allow the definition of distinct laminar, transitional, and turbulent regions. Comparison is made also with measurements of the structure and thickness growth of the boundary layer. These observations were made with controlled variations in the wall temperature ratio, nose bluntness and unit Reynolds number. A discussion is presented of the influence of these parameters on transition and comparison made with recent results in other facilities.		
<b>KEY WORDS</b> Boundary layer transition Hypersonic Experimental		

BY CUTTING OUT THIS RECTANGLE AND FOLDING ON THE CENTER LINE, THE ABOVE INFORMATION CAN BE FITTED INTO A STANDARD CARD FILE

AUTHOR

*E. J. Softley*

COUNTERSIGNED